Glass Ceramic Phosphors: Towards Long-Lifetime High-Power White Light-Emitting-Diode Applications–A Review

*Hang Lin, Tao Hu, Yao Cheng, Mingxiang Chen, and Yuansheng Wang**

With the technological advancements of high-quality lightings and high-end displays, white light-emitting-diodes (w-LEDs) are quickly developing towards high energy density excitation, high output power and high device stability, which requires outstanding thermal properties of the phosphor color converters. In this connection, all-inorganic luminescent glass ceramic (GC), exhibiting excellent physical/chemical stability to address the serious aging and yellowing issues of conventional phosphor/silicone composite, receives great attention recently and is regarded as a new generation color converter with longevity. Herein, a thorough survey of the research progress of this kind of material is made, with focus put on the design principle, microstructure-property relationship, packaging technology and the burgeoning application direction. Some challenging issues are discussed and potential directions are suggested for further developing the phosphor-glass composite fulfilling various requirements in practical application. This Review can promote rapid progress of long-lifetime high-power w-LEDs.

1. Introduction

Phosphor-converted white light-emitting-diodes (w-LEDs), showing extraordinary advantages of high luminescence efficiency, low power consumption, long operation life and environmental friendliness, have gradually replaced the conventional incandescent and fluorescent lamps, and will definitely dominate the future lighting market.[1–6]

State-of-the-art w-LED technology is rapidly developing towards "high-power" (≥1 W) to meet the increasing demand of high-brightness lighting in car headlamp, tunnel lamp, high-pole lamp, and floodlight projector, etc. (**Figure 1**) As known, the junction temperature of high-power w-LED on state can reach up to 150–200 °C, which poses strict requirements on the thermal properties of employed encapsulant.[7,8] The conventional organic silicone or resin with low thermal conductivity (0.1–0.2 W/mK) and poor thermal stability unavoidably suffers from serious yellowing and aging issues under such harsh heat environment, resulting in luminous efficacy (LE) degradation and color shifting after long-term use. The researchers in industrial and academic circles then devoted themselves to developing the all-inorganic phosphor color converter, e.g., rare earth ion (REI) doped glass, YAG: Ce^{3+} ceramics and YAG: Ce^{3+} glass ceramics (GC). REI doped glass possesses the advantages of high tolerance of REI doping, good homogeneity, moderate thermal conductivity (≈1 W/mK),[9] and insignificant photon scattering; unfortunately, its low quantum efficiency, arising from high phonon energy of the glass matrix, makes it far away from practical application. YAG: Ce^{3+} ceramics have good thermal conductivity of 5–13 W/mK,[10–12] and admirable luminescent properties especially when they are made into transparent (transmittance: 70–87% at 800 nm[11]). However, the tedious preparation procedure and the critical synthetic requirement (typically prepared under ≈1800 °C in vacuum) greatly increase the cost of transparent ceramic (TC) in mass production; in addition, the species of TC is rather few. As an alternative, YAG: Ce^{3+} GC, a composite material with YAG: Ce^{3+} crystals embedded in the amorphous glass matrix, has received growing interests recently.[13] GC combines both the merits of glass host and phosphor: not only the excellent luminescent behavior of phosphor can be retained, but also the admirable chemical and mechanical stability related to the glass matrix are gained. After optimizing the glass composition to make refractive index (RI, n) of the glass matrix and the embedded YAG: Ce^{3+} close to each other, the obtained GC could possess high transparency (≈80% at 800 nm).[8] Though the thermal conductivity of the YAG: Ce^{3+} GC (≈1 W/mK)[9] is somewhat inferior to that of the YAG: Ce^{3+} TC, it is still acceptable for most of the high-power application. Impressively, the low cost and the easy fabrication of GC favor its large-scale industrial production, and the plentiful species of GC allows fruitful emissive colors. Tanabe et al. firstly reported YAG: Ce^{3+}

Dr. H. Lin, T. Hu, Dr. Y. Cheng, Prof. Y. Wang
CAS Key Laboratory of Design and Assembly of Functional Nanostructures
and Fujian Key Laboratory of Nanomaterials
Fujian Institute of Research on the Structure of Matter
Chinese Academy of Sciences
Fuzhou, Fujian 350002, China
E-mail: yswang@fjirsm.ac.cn
Prof. M. Chen
School of Mechanical Science and Engineering
Huazhong University of Science and Technology
Wuhan 430074, China

The ORCID identification number(s) for the author(s) of this article can be found under https://doi.org/10.1002/lpor.201700344

DOI: 10.1002/lpor.201700344

Hang Lin is an associate professor of Fujian Institute of Research on the Structure of Matter (FJIRSM), Chinese Academy of Sciences (CAS). He received his bachelor, and master degrees from Fuzhou University (China), and PhD degree from FJIRSM, CAS, in the years of 2005, 2008, 2011, respectively. His current research interests include luminescent glass ceramics, phosphors, and w-LED devices.

Yao Cheng obtained his PhD degree in physical chemistry in 2007 from University of Chinese Academy of Sciences. He worked in Stockholm University as a postdoctoral researcher from 2007 to 2009. He is currently an assistant professor in Fujian Institute of Research on the Structure of Matter, CAS. His current research interests focus on the photoluminescent functional nanomaterials.

Yuansheng Wang received his B.S. degree (1982) from University of Science and Technology of China (USTC), M.S. degree (1985) from Institute of Solid State Physics, Chinese Academy of Sciences (CAS), Ph.D. (1989) in Condensed Matter Physics from USTC, and worked in Laboratoire de Thermodynamique et Physi-co-Chimie Métallurgiques, CNRS, France as a research fellow in 1990–1991. He was a Professor of Materials Science at Fuzhou University since 1999, and moved to Fujian Institute of Research on the Structure of Matter (FJIRSM), CAS as a Research Professor since 2002, leading a group conducting investigations on optoelectronic functional materials.

GC for w-LED application via an in-situ glass crystallization.[14] Cheng et al.[15] and Chung et al.[16] respectively reported YAG: Ce^{3+} GC via a low temperature co-sintering method, also named as "phosphor-in-glass" (PiG) approach, to combine phosphor particles and low-melting glass together at <1000 °C. Utilizing the PiG approach, in 2014, our group announced a record of internal QE (93%) for the YAG: Ce^{3+} GC and a record of LE (124 lm/W) for the GC-based w-LED under 350 mA driving current.[8] **Table 1** lists comparison of the properties associated with the criteria for solid-state lighting among REI doped glass, TC and GC. Under full consideration of the balance in cost, physical properties, and luminescent behaviors, GC is believed to be the most appropriate candidate for high-power w-LED application.

In view of more and more researchers have paid their attentions to GC for achieving longevity in high-power w-LED application, a review article on the design, preparation, structure, and luminescent properties of GC, as well as the photometric-chromaticity performance of corresponding GC-based w-LEDs is quite necessary. Previously, Prof. Chen published a mini-review, mainly concerning the synthesis and luminescence property of GC.[17] Herein, we try to make a more comprehensive survey and put more insights into the design principle and the structure-property relationship in GC. Some new progresses, e.g., GC-based warm w-LEDs, alternative current (AC) driven w-LED, and white laser diodes (w-LD) will be highlighted. The related challenges and perspectives will also be pointed out.

2. Design and Synthesis of GC for High-Power w-LEDs

2.1. Basic Design Principles

Phosphor and amorphous glass matrix are two basic functional units in GC. The former one endows the GC with luminescence property, and the latter one provides a stabilizing scaffold for accommodating the luminescent crystals. Therefore, the elaborate design or careful selection of these two components is the key to attaining desirable properties in GC.

So far, there have been many approaches, including crystal-site engineering, mixing of nanophases, single crystal growth, single-particle diagnosis, and solid state combinatorial chemistry, to design new phosphor to fulfill spectral requirements for diverse w-LED application directions.[18] Among the numerous phosphors reported hitherto, Eu^{2+} and Ce^{3+} activated phosphors are regarded as the most appropriate candidates, due to the following reasons:[4] 1) the $4f^n \leftrightarrow 4f^{n-1}5d^1$ transitions of Eu^{2+}, Ce^{3+} are parity-allowed (Laporte's selection rule is obeyed), which determines their high oscillator strengths (intense absorption and emission); 2) Eu^{2+} and Ce^{3+} exhibit adjustable luminescence dependent on the host, owing to the outer 5d electron is strongly affected by the local coordination environment; and 3) the short decay time of Eu^{2+} and Ce^{3+}, typically in the range of hundreds and tens of nanoseconds, greatly reduces the saturation effects. Eu^{3+} activated phosphor also receives great attentions, since Eu^{3+} can yield red luminescence with high QE when doping into an appropriate host.[19] Non-rare-earth Mn^{4+} activated oxide/fluoride red phosphors are known for their low cheap and narrow-band spectral profiles.[20–24] Besides, quantum dots (QDs), prized for the unique optoelectronic properties, are very suitable for w-LED backlight displays.[25] Incorporating the above mentioned phosphors into an appropriate glass matrix is one of the basic design principles.

There are two main strategies to achieve GC, including the precipitation of luminescent crystals via glass crystallization and the introduction of synthesized phosphor particles into glass matrix via low-temperature co-sintering, which require different glass chemistry knowledge to optimize luminescent performance of GC via the glass composition design.

For the former strategy, nucleation and crystal growth are two fundamental stages of crystallization in glass. Achieving vast homogeneous nucleation followed by uniform crystal growth in a controlled manner is of great importance;[26] since only when the precipitated crystallites are in the range of nanometers, smaller than the wavelength of visible light, the obtained GC can be made transparent (the scattering intensity is sixth power of particle size, according to Rayleigh scattering theory). High-transparency

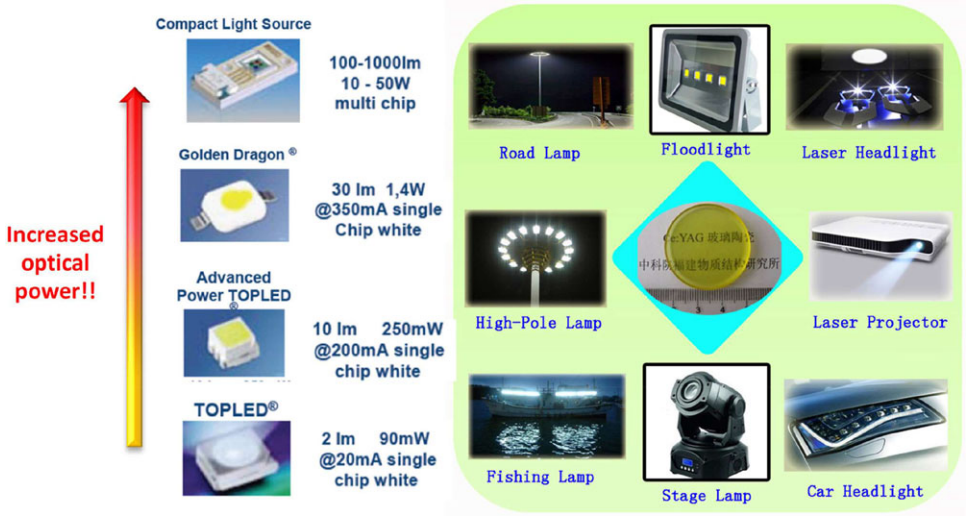

Figure 1. Schematical illustration of the all inorganic luminescent glass ceramic for high-power lighting or display applications.

Table 1. Comparison of the properties that associated with the criteria for w-LED among the REI doped glass, YAG: Ce TC and YAG: Ce GC.

	REI-doped glass	Transparent ceramics	Glass ceramics
PROS	• good homogeneity • high tolerance of REI doping • fruitful color • high transparency (no interface) • chemically/thermally stable • moderate thermal conductivity (≈1 W/mK) • low cost • easy fabrication	• good homogeneity • high transparency (70-87% at 800 nm) • high thermal conductivity (5-13 W/mK) • high quantum efficiency (>90%) • chemically/thermally ultra-stable	• semitransparent/transparent (up to 80% at 800 nm) • plentiful species and fruitful color • moderate thermal conductivity (≈1 W/mK) • high quantum efficiency (>90%) • chemically/thermally stable • low cost • easy fabrication
CONS	• low quantum efficiency • nonideal excitation wavelength/spectral profile • high synthesis temperature	• expensive • tedious preparation procedure • critical synthetic requirement (≈1800 °C in vacuum) • limited species • not easy processing	• difficult to homogenize phosphor particle distribution

is beneficial to improving luminescent performance of GC. In comparison with the glass matrix, the precipitated crystal provides a more appropriate crystalline environment for the optically active REIs, resulting in much improved luminescence efficiency. The key points to partition REIs into the precipitated crystal are the ionic radius matching and the charge balance between the REIs and the substituted cation of crystal.[28–30] Viewing that glass is a complex multicomponent system with the order of glass network differing in short, medium and long range, it is rather difficult to establish the relationships among glass composition, glass structure and glass crystallization process. And so there is no definite glass composition design principle followed to precipitate the target luminescent crystalline phase, let alone to achieve high transparency and effective REIs' doping. Many trial-and-error experiments are obligatory to be done. However, in some situations empirical considerations of glass composition are helpful. **Table 2** summarizes some commonly used glass components, their roles acted in glass network, as well as their functions, all of which should be considered when performing the glass composition design.[27]. The glass phase diagram model and the phase equilibria diagram should also be referred to gain knowledge of the tendencies toward glass crystallization or phase-separation.

For the latter strategy, in order to gain a good luminescent performance, GC should be transparent, and glass component should exhibit low chemical activity and high thermal stability: they should not react with phosphor particles, and should not perform crystallization as well, during the glass-phosphor co-sintering. To this end, several factors need to be considered, for examples: 1) the refractive index of glass should be designed to match with that of the embedded phosphor particles for high transparency, according to the Mie theory (**Figure 2**); 2) the density of glass melt should be close to that of phosphor particles for preventing particle agglomeration which may induce photon scattering; and 3) the number of non-bridging oxygens (NBOs) in glass should be finely controlled to a limited level, considering NBOs have a high electron density to react with the embedded phosphor particles.[31]

Table 2. Commonly used glass compounds, their roles acted in glass network and their functions.[27]

Composition	Role	Function
SiO_2	glass network former	increasing hardness, thermal/chemical stability, melting temperature, and viscosity; probably inducing crystallization
Al_2O_3	glass network intermediate	increasing hardness, thermal/chemical stability, melting temperature, and viscosity; reducing crystallization tendency;
B_2O_3	glass network former	reducing viscosity at high temperature; increasing viscosity at low temperature; accelerating glass clarification and homogenization
P_2O_5	glass network former	reducing viscosity; increasing thermal expansion coefficient; prejudicing chemical stability
Na_2O	glass network modifier	reducing melting temperature (good flux), viscosity, and thermal/chemical stability;
K_2O	glass network modifier	similar to Na_2O; increasing transparency; reducing crystallization tendency
BaO	glass network modifier	increasing refractive index and density, flux
ZnO	glass network intermediate	stabilizing glass network; reducing thermal expansion coefficient; increasing refractive index and thermal/chemical stability
La_2O_3	glass network modifier	increasing refractive index, reducing chromatic dispersion; increasing chemical stability
TiO_2/ZrO_2	glass network modifier	nucleation agents

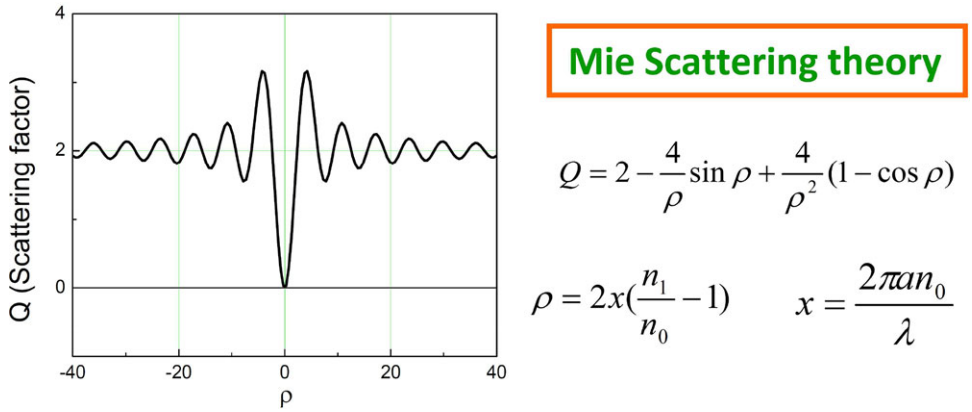

Figure 2. Dependence of scattering factor Q on ρ, according to Mie scattering theory (n_0 and n_1 are the RI of medium and scatterer, respectively; a is the radius of scatterer, and λ is the wavelength of the incident light).

The calculation method proposed by Prof. Gan can serve as a guide to attain the expected refractive index and density in glass:[32]

$$G = \sum g_i r_i \quad (1)$$

where G is the physical property, g_i is the partial property with respect to the component i in the glass, and r_i is the molar concentration of the component in the glass. The importance of glass composition design to obtain good optical properties in GC was demonstrated in our group.[33] It is found that the GC prepared via PiG route possesses high transparency only when RI and density of the glass match with those of the embedded YAG: Ce^{3+}, Mn^{2+} (Sample 2 in **Figure 3**).

The number of NBOs can be effectively adjusted by varying the glass composition. Taken the Na_2O-B_2O_3-SiO_2 glass as an example,[34] the number of NBOs reduces when the Na_2O content decreases. The ^{11}B NMR results reveal that the glass structure is dependent on the molar ratios of $R = Na_2O/B_2O$ and $K = SiO_2/B_2O_3$. For $R \leq 0.5$, Na^+ ions are attracted primarily by the borate network. For $R > 0.5$, the addition of one molecule of Na_2O results in the formation of four $[BSi_4O_{10}]^{-1}$ units at the expense of one diborate unit and sixteen SiO_4 units. Particularly, for $1/2 + K/16 \leq R \leq 1/2 + K/4$, all additional Na_2O is employed in forming NBOs on the silica tetrahedral; and for $1/2 + K/4 \leq R \leq 2 + K$, the additional Na_2O destroys the reedmergnerite groups and forms pyroborate units and silica tetrahedrals with two NBOs per Si atom.

2.2. Synthesis Methods

At present, the synthesis methods of GC include glass crystallization, low temperature co-sintering, screen-printing, tape-casting, sol-gel, and spark plasma sintering (SPS).

- Glass crystallization

This is one of the most widely used methods to synthesize GC, and its process includes: mixing and grinding various raw materials in a certain proportion; making the mixture melt in a muffle furnace; quickly pouring the molten liquid into mold to obtain the precursor glass; and finally treating the precursor glass at a certain temperature to induce glass crystallization (**Figure 4**).

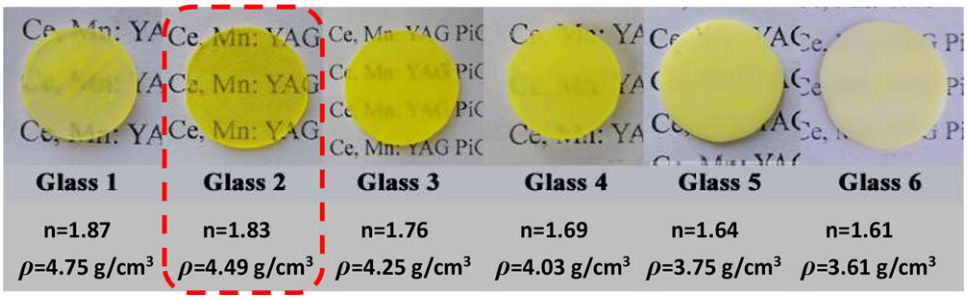

Figure 3. Photographs of the YAG: Ce^{3+}, Mn^{2+} microcrystals embedded GC prepared based on the precursor glasses in different RIs and densities. Reproduced with permission.[33] Copyright 2015, Royal Society of Chemistry.

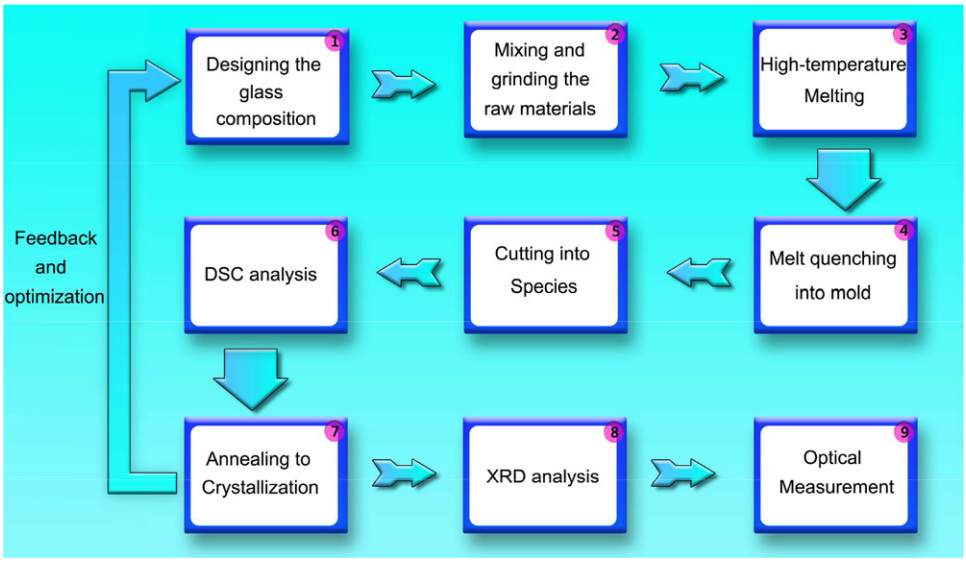

Figure 4. Flow chart of GC preparation via glass crystallization route.

The greatest advantage of this method is high-transparency obtained in the GC. Selecting appropriate annealing history to control nucleation and crystal growth in glass is important to achieve high transparency; otherwise the severer structural rearrangement may occur above the glass transition temperature, resulting in destruction of the glass network (i.e., devitrification). The other great advantage is that it can follow the matured glass manufacturing process, such as, pressing, rolling, drawing, and casting, which is helpful to fabricate GC in irregular forms and to put it into mass production. Nevertheless, the deficiency of this method is also obvious: the glass composition tends to deviate due to heat treatment at an ultra-high temperature; the crystallization fraction is usually low; some specified crystalline phases are hard to be precipitated; and REI is difficult to be totally partitioned into crystalline phases.

- Low temperature co-sintering (PiG)

Unlike glass crystallization, phosphor particles are directly blended and then melted with glass frit at low temperature (<1000 °C) by using the low temperature co-sintering route (**Figure 5**). This route is also called as "PiG". According to the difference in processing procedure, PiG falls into two categories: the re-melting method and the tableting-sintering method. The former one applies to TeO_2-, Sb_2O_3-, or Bi_2O_3-based GC, where the glass melting temperature is low and the melt possesses good fluidity that allows melt-quenching again. The latter one applies to SiO_2-based GC, where the phosphor and glass powders have to be compressed into a form of disk and then co-sintered above glass transition temperature (or at softening temperature) to combine them together. The GC prepared based on the PiG strategy, called as PiG color converter, exhibits superior luminescent behaviors and good flexibility to control color, since almost all kinds of up-to-date phosphors can be introduced into glass matrix. Moreover, it is praised for the merits of facile fabrication and the possibility of large-scale production.

- Screen-printing

Screen printing has been extensively used for microelectronics and the packaging of passive components, but only in more recent years did it apply to the phosphor-glass color converter for w-LEDs, firstly reported by Yang et al.[35] **Figure 6** schematically illustrates the preparation route of screen printing, i.e., an ink paste, made of phosphor, glass, organic solvent, and adhesives, is coated on the surface of glass plate by using a squeegee, followed

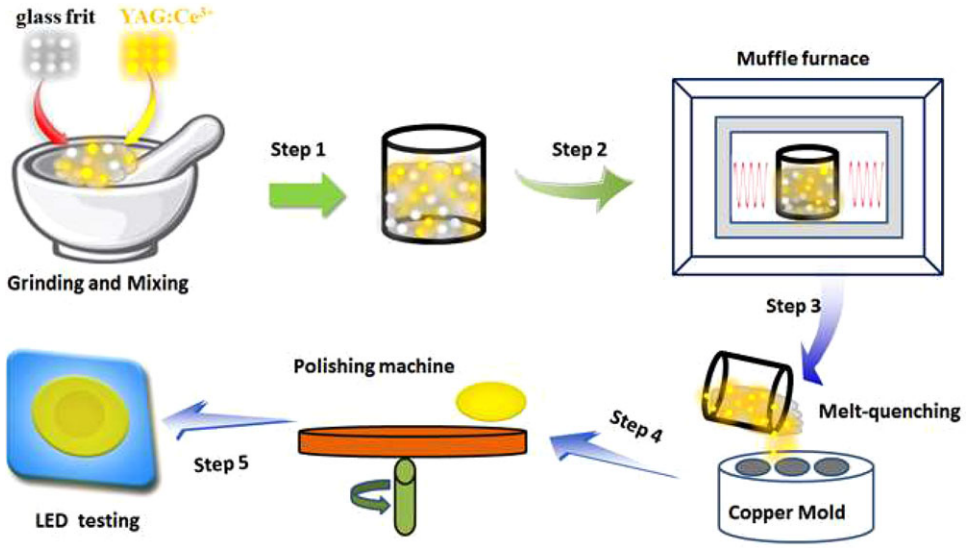

Figure 5. Schematic illustration of GC preparation via low-temperature co-sintering route.

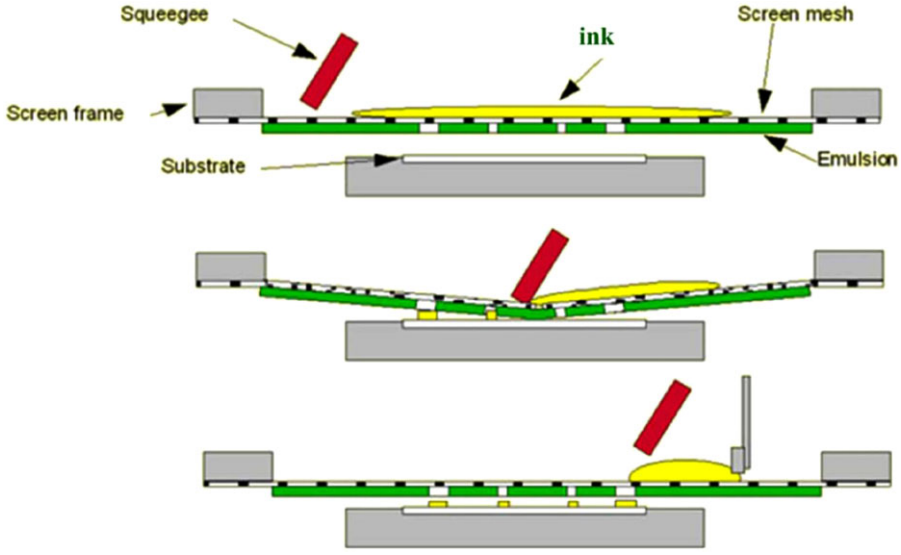

Figure 6. Schematic illustration of GC preparation via screen-printing route. Reproduced with permission.[35] Copyright 2013, American Optical Society.

by drying and sintering the composite. Essentially, the obtained product can still be called as PiG color converter, so this method has the same advantage as PiG method. Considering the coating can be structured by alternating or stacking phosphor layers of different composition, width, or thickness, it offers opportunity to design w-LED package in a smarter way.

- Tape-casting

Tape-casting is a well-established technique used for large-scale fabrication of ceramic. Wang et al. firstly adopted this method to fabricate PiG color converter (**Figure 7**).[36] In a typical procedure, the glass and phosphor powders are ball-milled with dispersant, binder and plastic agent in ethanol and xylene for 24 h into slurry. The slurry is then coated on a substrate glass by using a doctor blade, followed by laminating under a proper pressure and sintering at a proper temperature. This method allows the automated production of GC. The precise thickness control from several to hundreds micrometers can be achieved by adjusting chemical composition, blade height and sintering process, without additional polishing.

- Sol-gel

Glass can be obtained by the sol-gel method, in which the metal alkoxides are hydrolyzed and condensed in a solution. After heat treatment, it is possible to precipitate the target phosphor with the partition of activators into crystals. Segawa *et al.* proposed the other way,[37] i.e., introducing phosphors into sol during the reaction, and then calcining the gel at an appropriate temperature to form PiG color converter. This method allows good homogeneity of the product and easy compositional

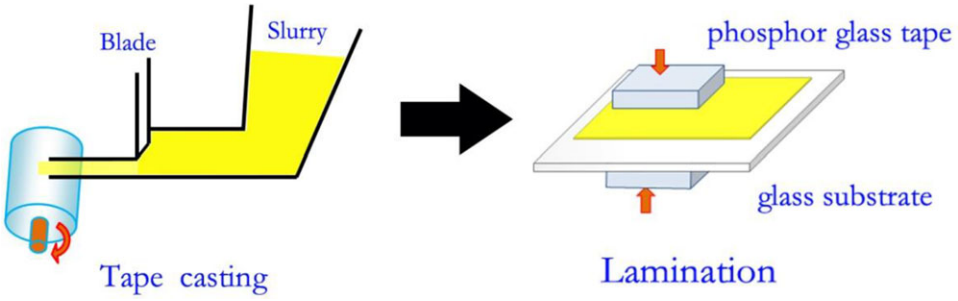

Figure 7. Schematic illustration of GC preparation via tape-casting route.[36]

control; however, the process is time-consuming, the residual carbon/hydroxyl groups have adverse impact on the optical properties of GC, and it is also difficult to fabricate the large bulk samples owing to the cracks formed during solvent evaporation.

- SPS

Spark plasma sintering (SPS) is an advanced technology to fabricate ceramics. Recently, Zhou et al. reported the fabrication of GC embedded with YAG:Ce crystals by using this method,[38] demonstrating its ability of achieving fully dense glass materials at a comparatively low temperature within a very short time.

As presented in **Table 3** below, the optical properties of GC and GC-based w-LED rely on the synthesis process. The GC synthesized via glass crystallization route exhibits the poorest luminescence performance, probably ascribing to the diffculty to partition all active ions into the precipitated particles and the luminescence quenching by defects (which are induced by the ion diffusion between phosphor particles and glass matrix for the high crystallization temperature). The optical properties of GC prepared via the sol-gel route are injured by the residual carbon/hydroxyl groups. As for the GC prepared by screen-printing or tape-casting, the abundant pores, induced by the evaporation of organic binder, serve as adverse scattering centers, and so, they exhibit moderate luminescence performance. Remarkably, the GC synthesized by using the low-temperature co-sintering method can yield quantum efficiency higher than 90% and lumious efficacy up to 120–130 lm/W, after optimizing glass composition and preparation procedure. These admirable optical properties originate from those of the original elaborately-prepared phosphor particles which can withstand glass-melting without thermal degradation.

3. Structure-Property Relationship

Establishing structure-property relationship is of great significance to improve the luminescent performance of GC and GC-based w-LEDs. There have been some endeavors paid to study the structure-property relationship in GC via glass composition adjustment, phosphor pre-treatment, and glass preparation procedure optimization.

Shyu et al. studied the effect of YAG:Ce^{3+} prenitridizing treatment on the glass-phosphor reactions and the resulting luminescence properties of YAG:Ce^{3+} PiG color converter based on the glass system of Bi_2O_3-B_2O_3-ZnO-Sb_2O_5 (BiG). [39] In the study, a high-T_g silicate glass (SiG) was also used for comparison. It is found the BiG glass retains more phosphor phase (83%–87%) than that (78%–82%) using the SiG glass, due to the lower co-sintering temperature. Moreover, replacing YAG:Ce^{3+} (Y) by nitridized YAG:Ce^{3+} (NY) for both glass matrices increase the phosphor phase content by ≈4%. The retained phosphor phase content can be further improved to 97.5% in the BiG glass when using nitrogen instead of air as the sintering atmosphere. The suppression of phosphor-glass reaction should be responsible for this phenomenon, as confirmed by TEM analyses (**Figure 8**a–d). According to the contrast differences in the TEM images and the EDS results, at least three layers (denoted as 1, 2, and 3) exist between the phosphor and the glass, and the region *a-b-c-d-e* constitutes the reaction zone (Figure 8e). It is demonstrated that Bi shows the strongest tendency to react with phosphor, followed by Zn, whereas B and Sb the weakest. As a comparison, the SiG glass exhibits more serious corrosion than the BiG glass (Figure 8f,g), with the region *m-n-o-p*-q-*r-s* as the reaction zone (Figure 8h). Ca, Si, and Na tend to diffuse from glass toward YAG during sintering, among which Ca has a faster diffusion rate than Na and Si. Increasing the degree of nitridizing treatment by using prenitridized YAG and N_2 sintering atmosphere reduce the degree of reaction, and in turn increase the emission intensity of GC to ≈1.8%.

The degree of phosphor-glass reaction also strongly relies on the sintering temperature of PiG color converter, as demonstrated by Chen et al.[40] HRTEM observations (**Figure 9**a–c) show a diffusion zone of 5–40 nm between the YAG:Ce^{3+} particles and the glass matrix (SiO_2-Na_2O-Al_2O_3-CaO) when prepared at 800–900 °C, while no such diffusion zone for the sample sintered at 700 °C. SAED patterns taken on the interface between YAG and SiO_2 clearly show the distinguishable crystalline spots, indicating the corrosion effect is insignificant at 700 °C; in contrast, both the diffraction spots and amorphous rings are observable at 800–900 °C, suggesting the occurrence of inter-diffusion. EDS analyses reveal a much stronger inter-diffusion between Si and Al atoms at a higher sintering temperature. As expected, the luminescent performance of YAG:Ce^{3+} GC prepared at lower temperature is much better. The similar results are found in the CASN:Eu^{2+} GC (Figure 9d–f).[41]

Segawa et al. made a comparison between the GCs fabricated by introducing α-SiAlON into Na_2O-ZnO-B_2O_3 and Na_2O-ZnO-TeO_2 glasses respectively, and pointed out that the tellurite glasses might have reacted more readily with the α-SiAlON, because the Te atoms easily react with oxygen for the lone electron pair on the Te atoms.[31] Herrmann et al. also demonstrated the addition of heavy metal ion can be chemically aggressive and

Table 3. Summary of the preparation route, material system, and luminescent property of GC.

Method	Glass matrix	Embedded phosphors	QE	LE [lm/W]	Application	Ref.
Glass crystallization	SiO_2-Al_2O_3-Y_2O_3	YAG:Ce^{3+}	30%		Blue-excited cool w-LED	[14]
	PbO-SiO_2-Al_2O_3-Y_2O_3-B_2O_3-CeF_3	YAG:Ce^{3+}	–	97 (20 mA)	Blue-excited cool w-LED	[48]
	CaO-SiO_2-Eu_2O_3	β-Ca_2SiO_4:Eu^{2+} $Ca_3Si_2O_7$:Eu^{2+}	–	–	Blue-excited cool w-LED	[49]
	SiO_2-Al_2O_3-LiF-YF_3-Ga_2O_3	γ-Ga_2O_3:Mn^{2+}+ β-YF_3:Tm^{3+}	–	–	UV-excited w-LED	[50]
	SiO_2-Al_2O_3-Y_2O_3-CaO-ZnO-Eu_2O_3	$CaAl_2Si_2O_8$:Eu^{2}+$Y_{20}Si_{12}O_{48}N_4$:Eu^{3+}	43.3%	–	UV-excited w-LED	[51]
	SiO_2-Al_2O_3-NaF-CeF_3	CeF_3:Dy^{3+}	–	–	UV-excited w-LED	[52]
	BaO-SiO_2	$BaSi_2O_5$:Eu^{2+}	–	–	UV-excited w-LED	[53]
	SiO_2-Al_2O_3-CaF_2-CeF_3-DyF_3	CeOF:Dy^{3+}	–	–	UV-excited w-LED	[54]
	SiO_2-Al_2O_3-Na_2CO_3-NaF-YF_3-P_2O_5-Eu_2O_3	YPO$_4$:Eu^{3+}	–	–	UV-excited w-LED	[55]
	SiO_2-B_2O_3-Na_2O-SrF_2-GdF_3	Sr_2GdF_7: Eu^{3+}/Tb^{3+}	–	–	UV-excited w-LED	[56]
	SiO_2-GeO_2-Al_2O_3-ZnO-K_2O-Na_2O	Ce^{3+}/Mn^{2+}: β-Zn_2SiO_4	–	–	UV-excited w-LED	[57]
	SiO_2-Na_2O-Al_2O_3-LaF_3	LaF_3:Eu^{2+}/Eu^{3+}	–	–	UV-excited w-LED	[58]
	SiO_2-B_2O_3-RO (R = Ba, Zn)	YAG:Ce^{3+}	–	–	Blue-excited cool w-LED	[16]
Low-temperature co-sintering (Tableting-sintering)	SiO_2-B_2O_3-RO-Eu_2O_3/Pr_2O_3 (R = Ba, Zn)	YAG:Ce^{3+}	–	–	Blue-excited cool/warm w-LED	[59]
	SiO_2-B_2O_3-RO (R = Ba, Zn)	Ca-α-SiAlON:Eu^{2+}	–	88 (350 mA)	Blue-excited warm w-LED	[47]
	SiO_2-Na_2O-RO(R = Ba, Zn)	CASN:Eu^{2+} + YAG:Ce^{3+}	–	–	Blue-excited warm w-LED	[60]
	SiO_2-B_2O_3-ZnO-Na_2O	CASN:Eu^{2+} + YAG:Ce^{3+}	–	–	Blue-excited warm w-LED	[61]
	SiO_2-B_2O_3-ZnO-Al_2O_3-K_2O	CASN:Eu^{2+} + LuAG:Ce^{3+}	–	≈25	Blue-excited cool/warm w-LED	[62]
	SiO_2-B_2O_3-ZnO-Al_2O_3-K_2O	$SrGa_2S_4$:Eu^{2+} + CASN:Eu^{2+}	–	–	Blue-excited cool/warm w-LED	[63]
	SiO_2-B_2O_3-ZnO-Al_2O_3-K_2O	YAG:Ce^{3+} ($CuInS_2$/ZnS QDs coating on PiG)	–	3.7 (20 mA)	Blue-excited cool/warm w-LED	[64]
	SiO_2-B_2O_3-ZnO-Al_2O_3-K_2O	CASN:Eu^{2+} + LuAG:Ce^{3+}	–	5–8 (350 mA)	Blue-excited cool/warm w-LED	[65]
	SiO_2-B_2O_3-ZnO-Al_2O_3-K_2O	$SrGa_2S_4$:Eu^{2+} (PiG cuts into micro-tube)	–	–	Blue-excited warm w-LED	[66]
	SiO_2-P_2O_5-ZnO-B_2O_3-R_2O (R = K and Na)	YAG:Ce^{3+} + CASN:Eu^{2+}	–	77.6–103.7 (20 mA)	Blue-excited cool/warm w-LED	[67]

(*Continued*)

Table 3. Continued.

Method	Glass matrix	Embedded phosphors	QE	LE [lm/W]	Application	Ref.
	PbO-B_2O_3-SiO_2-MnO PbO-B_2O_3-SiO_2-Eu_2O_3	YAG:Ce^{3+}	–	–	Blue-excited cool/warm w-LED	[68]
	PbO-B_2O_3-SiO_2-Eu_2O_3	CASN:Eu + β-SiAlON:Eu + $Sr_5(PO_4)_3Cl$:Eu	–	58.4	UV-excited warm w-LED	[69]
	SiO_2-Na_2O-Al_2O_3-CaO	YAG:Ce^{3+}	68%	–	Blue-excited cool w-LED	[40]
	SiO_2-Na_2O-Al_2O_3-CaO	YAG:Ce^{3+} + LuAG:Ce^{3+} CASN:Eu^{2+}	55.6%	–	Blue-excited warm w-LED	[41]
	SiO_2-Na_2O-Al_2O_3-CaO	YAG:Ce^{3+} + YAG:Tb^{3+} CASN:Eu^{2+}	55.6%	–	Blue-excited warm w-LED	[70]
	B_2O_3-Bi_2O_3-Al_2O_3-ZnO	YAG:Ce^{3+} + CASN:Eu^{2+}	58%	–	Blue-excited warm w-LED	[71]
	Na_2O-CaO-SiO_2	YAG:Ce^{3+}, LuAG:Ce^{3+}	–	–	Blue-excited cool w-LED	[42]
	Na_2O-CaO-Al_2O_3-SiO_2	LuAG:Ce^{3+}@SiO_2	71%	≈130 (500 mA)	Blue-excited cool w-LED	[43]
	SiO_2-Al_2O_3-Na_2O-CaO-Eu_2O_3	$Sr_4Al_{14}O_{25}$:Eu^{2+}	60.4%	–	Blue-excited warm w-LED	[72]
	ZnO-B_2O_3-BaO-Al_2O_3	β-SiAlON:Eu^{2+}	29% (external)	–	Blue-excited LD	[73]
	ZnO-B_2O_3-BaO-Al_2O_3	CASN:Eu^{2+}	43% (external)	–	Blue-excited LD	[74]
	SiO_2-Al_2O_3-B_2O_3-ZnO-BaO	$Ca_9Gd(PO_4)_7$:Eu^{2+},Mn^{2+}	26.2%	–	UV-excited warm w-LED	[75]
	SiO_2-Al_2O_3-B_2O_3-ZnO-BaO	YAG:Ce^{3+} + MMG:Mn^{4+}	≈70%	42–102 (300 mA, LED); 110 (LD)	Blue-excited warm w-LED/LD	[76]
Low-temperature co-sintering (re-melting)	R_2O-ZnO-B_2O_3 (R = Li, Na, K); NaO-ZnO-TeO_2	Ca-α-SiAlON:Eu^{2+}	–	–	Blue-excited w-LED	[31]
	MO-P_2O_5 (M = Zn, Ca, Ba)	Ca-α-SiAlON:Eu^{2+}	≈50% (external)	–	Blue-excited w-LED	[77,78]
	Na_2O-B_2O_3-SiO_2	Ca-α-SiAlON:Eu^{2+}	≈50% (external)	–	Blue-excited w-LED	[34,79]
	Sb_2O_3-B_2O_3-TeO_2-ZnO-Na_2O-La_2O_3-BaO	YAG:Ce^{3+}	92%	124.6 (350 mA)	Blue-excited cool w-LED	[8]
	Sb_2O_3-B_2O_3-TeO_2-ZnO-Na_2O-La_2O_3-BaO	$CaMg_2Al_{16}O_{27}$:Mn^{4+} + YAG:Ce^{3+}	33.8% for red PiG	124–58 (350 mA)	Blue-excited cool/warm w-LED	[80]
	TeO_2-B_2O_3-ZnO-Na_2O-Al_2O_3	$BaMgAl_{10}O_{17}$:Mn^{4+}, Mg^{2+} + YAG:Ce^{3+}	–	99.2–55.1 (350 mA)	Blue-excited cool/warm w-LED	[81]
	TeO_2-B_2O_3-ZnO-Na_2O-Al_2O_3	YAG:Ce^{3+}, Mn^{2+}, Si^{4+}	85.6%–32.2%	106–40 (350 mA)	Blue-excited cool/warm w-LED	[33]
	TeO_2-B_2O_3-ZnO-Na_2O	$Y_3Mg_2AlSi_2O_{12}$:Ce^{3+} + YAGG:Ce^{3+}	93.2% for green PiG	62–32 (350 mA)	Blue-excited cool/warm w-LED	[82]
	Sb_2O_3-B_2O_3-TeO_2-ZnO-Na_2O-La_2O_3-BaO	GdAGG:Ce^{3+} + YAG:Ce^{3+}	89.4%	82 (350 mA)	Blue-excited AC-LED	[83]
	Sb_2O_3-ZnO-K_2O-B_2O_3	YAG:Ce^{3+}	94%	130 (350 mA)	Blue-excited cool w-LED	[84]
	Sb_2O_3-B_2O_3-TeO_2-ZnO-Na_2O-La_2O_3-BaO	$Li_6CaLa_2Sb_2O_{12}$:Eu^{3+} + YAG:Ce^{3+}	89.3%	101	Blue-excited cool/warm w-LED	[85]
	Sb_2O_3-B_2O_3-TeO_2-ZnO-Na_2O-La_2O_3-BaO-Eu_2O_3	YAG:Ce^{3+}	92.6%	70–137 (350 mA)	Blue-excited cool/warm w-LED	[86]
	Sb_2O_3-B_2O_3-TeO_2-ZnO-Na_2O-La_2O_3-BaO-Eu_2O_3	$La_2Ti_2O_7$:Eu^{3+} + YAG:Ce^{3+}	–	105 (20 mA)	Blue-excited cool/warm w-LED	[87]
	Sb_2O_3-B_2O_3-TeO_2-ZnO-Na_2O-La_2O_3-BaO-Eu_2O_3	$La_{0.5}Na_{0.5}TiO_3$ + YAG:Ce^{3+}	89.6%	109–89 (60 mA)	Blue-excited cool/warm w-LED	[88]

(*Continued*)

Table 3. Continued.

Method	Glass matrix	Embedded phosphors	QE	LE [lm/W]	Application	Ref.
	Sb_2O_3-B_2O_3-TeO_2-ZnO-Na_2O-La_2O_3-BaO-Eu_2O_3	YAG:Mn^{4+} + YAG:Ce^{3+}	–	–	Blue-excited warm w-LED	[89]
	Sb_2O_3-ZnO-K_2O-B_2O_3	YAG:Ce^{3+}, Mn^{2+}, Si^{4+} + YAG:Ce^{3+}	55%–65%	136–82 (350 mA)	Blue-excited warm w-LED	[90]
	Sb_2O_3-B_2O_3-TeO_2-ZnO-Na_2O-La_2O_3-BaO-Eu_2O_3	$SrMgAl_{10}O_{17}$: Mn^{4+}, Li^+ + YAG:Ce^{3+}	–	113–58 (60 mA)	Blue-excited warm w-LED	[91]
	SnO-SnF_2-P_2O_5	YAG:Ce^{3+}	–	118 (350 mA)	Blue-excited cool w-LED	[9]
	SnO-SnF_2-P_2O_5-MF (M = Li, Na, K)	YAG:Ce^{3+} + CASN:Eu^{2+}	–	65–80 (350 mA)	Blue-excited warm w-LED	[92]
	SnO-SnF_2-P_2O_5	YAG:Ce^{3+} + CASN:Eu^{2+}	88.6% for CASN:Eu	90.7 (350 mA)	Blue-excited warm w-LED	[93]
	PbO-B_2O_3-SiO_2-ZnO	YAG:Ce^{3+}	–	134 (60 mA)	Blue-excited cool w-LED	[94]
	TeO_2-ZnO-K_2O-B_2O_3-Bi_2O_3	YAG:Ce^{3+}	–	125 (20 mA)	Blue-excited cool w-LED	[95]
	PbO-B_2O_3-SiO_2-ZnO	YAG:Ce^{3+}	≈40%	112.8 (400 mA)	Blue-excited cool w-LED	[96]
Screen-printing	PbO-B_2O_3-SiO_2	YAG:Ce^{3+}	–	81.2 (350 mA)	Blue-excited cool w-LED	[35,97]
	B_2O_3-SiO_2-Al_2O_3	CASN:Eu^{2+}+$Ba_2MgSi_2O_7$:Eu^{2+}+$(Sr,Ba)_3MgSi_2O_8$:Eu^{2+}	–	≈27 (500 mA)	UV-excited w-LED	[98–100]
	B_2O_3-SiO_2	YAG:Ce^{3+} + CASN:Eu^{2+}	–	58.6 (350 mA)	Blue-excited warm w-LED	[101]
	B_2O_3-SiO_2-M_2O-RO-Al_2O_3 (M = Na, K, Li; R = Zn, Ba)	YAG:Ce^{3+}	–	40–50 (500 mA)	Blue-excited cool w-LED	[102–105]
	SiO_2-B_2O_3-ZnO-BaO-K_2O-Na_2O-Li_2O-Al_2O_3	YAG:Ce^{3+} + CASN:Eu^{2+}	–	58.6–69.9 (350 mA)	Blue-excited warm w-LED	[106]
	SiO_2-P_2O_5-ZnO-B_2O_3-R_2O	YAG:Ce^{3+} + CASN:Eu^{2+}	–	≈120 (20 mA)	Blue-excited warm w-LED	[107]
	Bi_2O_3−ZnO−B_2O_3	$(Ba,Sr,Ca)_2SiO_4$:Eu^{2+}	–	≈32 (200 mA)	Blue-excited w-LED	[108]
	Bi_2O_3−ZnO−B_2O_3	$Sr_2Si_7Al_3ON_{13}$: Eu^{2+} + $CaMgSi_2O_6$:Eu^{2+}	–	55 (200 mA)	Blue-excited warm w-LED	[109]
	SiO_2-B_2O_3-ZnO-Al_2O_3	SCASN:Eu^{2+}+ LuAG:Ce^{3+}	–	50–73	Blue-excited warm w-LED	[110,111]
	TeO_2-B_2O_3-ZnO-Na_2O-Al_2O_3	YAG:Ce^{3+}	–	78.7 (350 mA)	Blue-excited cool w-LED	[112]
	P_2O_5-ZnO-B_2O_3-BaO	YAG:Ce^{3+}	–	20–30 (500 mA)	Blue-excited cool w-LED	[113]
	TeO_2-Sb_2O_3-Al_2O_3-B_2O_3-Na_2O-ZnO	LuAG:Ce^{3+} (K_2SiF_6:Mn^{4+} coated)	–	88–105 (20 mA)	Blue-excited cool w-LED	[114]
	TeO_2-Li_2O-ZnO	YAGG:Ce^{3+} ($Ca_2Si_5N_8$:Eu^{2+} coated)	–	88–105 (20 mA)	Blue-excited warm w-LED	[115]
	TeO_2-Sb_2O_3-Li_2O-ZnO	LuAG:Ce^{3+} (CASN:Eu^{2+} coated)	–	109–90 (20 mA)	Blue-excited w-LED	[116]
Tape-casting	PbO-B_2O_3-SiO_2-ZnO	YAG:Ce^{3+}	–	87.4 (20 mA)	Blue-excited w-LED	[36]
	PbO-B_2O_3-SiO_2-ZnO	YAG:Ce^{3+}	–	108.5 (20 mA)	Blue-excited w-LED	[117]
	TeO_2-ZnO-Sb_2O_3-Al_2O_3-B_2O_3-Na_2O	YAG:Ce^{3+} (C-dot coated)	–	83-31 (20 mA)	Blue-excited warm w-LED	[118]
Sol-gel	SiO_2	Ca-α-SiAlON:Eu^2	40%–50%	–	Blue-excited w-LED	[119,120]
	SiO_2	β-SiAlON:Eu^{2+}	74.7%	–	Blue-excited LD	[121]
	SiO_2-TiO_2	Ca-α-SiAlON:Eu^2	80%–90%	–	Blue-excited w-LED	[122]
SPS	SiO_2	YAG:Ce^{3+}	93.5%	127.9 (20 mA)	Blue-excited cool w-LED	[38]

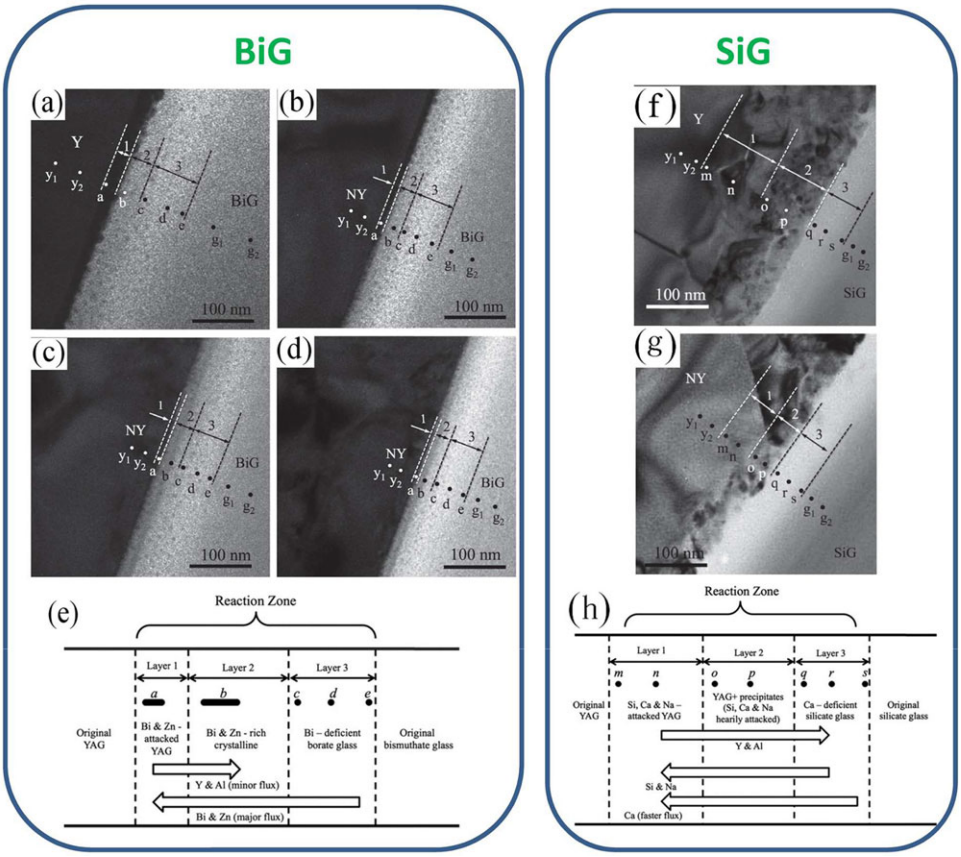

Figure 8. TEM bright-field images to show the interface regions between phosphor and glass with various heat-treatment conditions in a–d) BiG-GC and f,g) SiG-GC. Schematic diagrams to show the element distribution within the reaction zone in e) BiG- and h) SiG-GCs. Reproduced with permission.[39] Copyright 2016, Wiley-VCH.

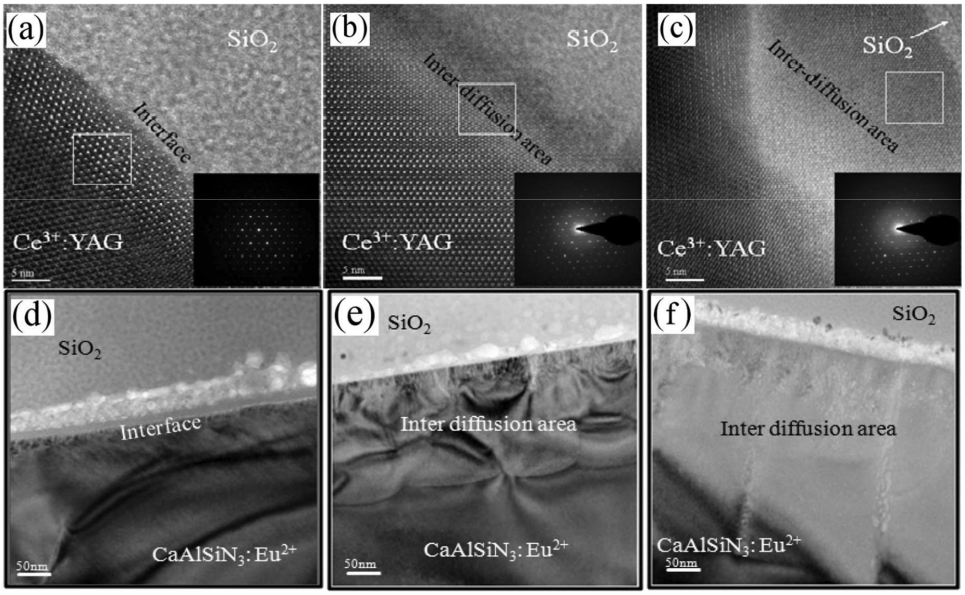

Figure 9. HRTEM images of the YAG:Ce^{3+} GC samples prepared at a) 700 °C, b) 800 °C, and c) 900 °C; insets are the corresponding SAED patterns at the interface between YAG and SiO_2. Reproduced with permission.[40] Copyright 2013, American Optical Society. HRTEM images of the CASN:Eu^{2+} GC samples prepared at d) 680 °C, e) 700 °C, and f) 750 °C. Reproduced with permission.[41] Copyright 2014, American Optical Society.

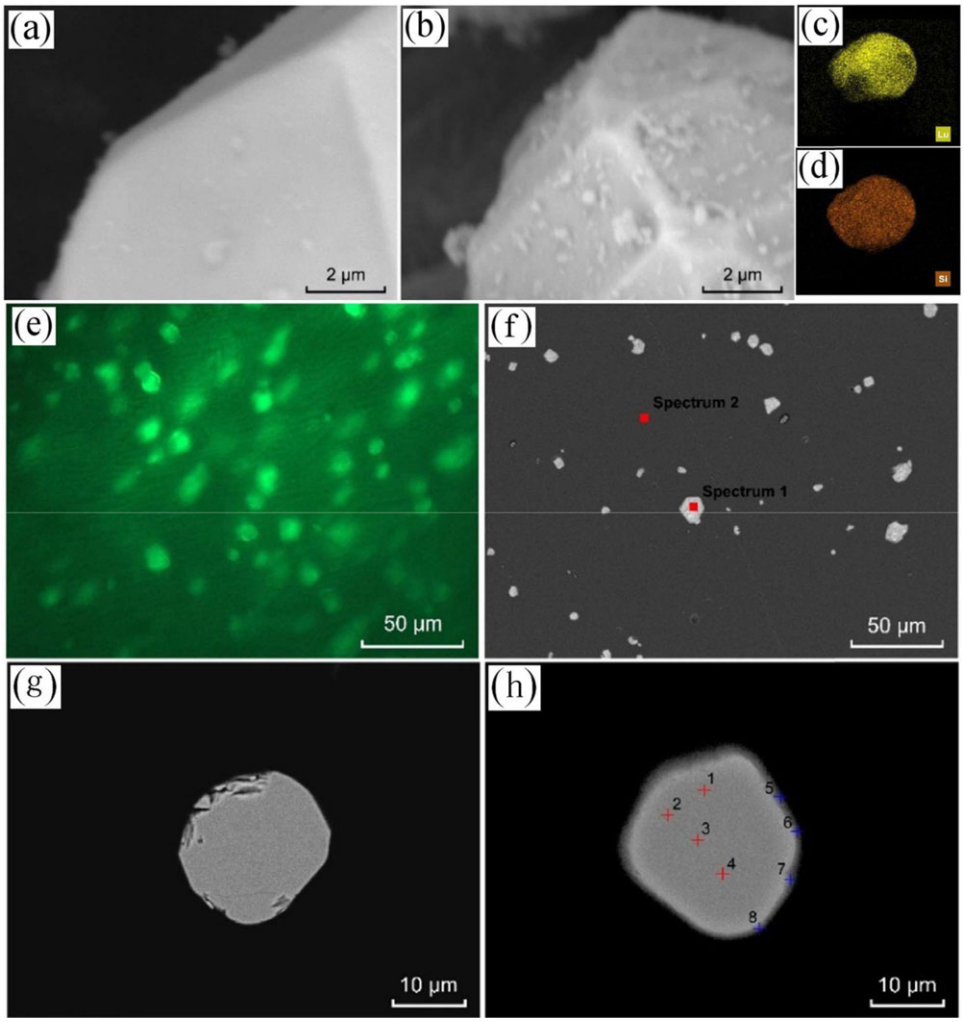

Figure 10. SEM images of a) uncoated, and b) 40 wt.% colloidal silica coated LuAG:Ce^{3+} phosphors. EDS mapping of an individual LuAG:Ce^{3+}@SiO_2 particle showing the typical signal of c) Lu and d) Si. e) Image observed using a micro-PL system with 355 nm laser as excitation source. f) Cross-sectional SEM micrograph of GC. g) Cross-sectional SEM micrographs of LuAG:Ce^{3+}@SiO_2 GC and h) pristine LuAG:Ce^{3+} GC. Reproduced with permission.[43] Copyright 2016, Elsevier.

dissolve the phosphor easily.[42] However, with the addition of heavy metal ion, the synthesis temperature is reduced and the refractive index of glass matrix is improved, which are beneficial to enhancing quantum efficiency and light extraction efficiency of the GC. Overall, the advantage outweighs the disadvantage in the aspect of luminescence performance.

Constructing the core-shell structure on phosphors via coating is hopeful to reduce the phosphor degradation during glass-phosphor co-sintering, as demonstrated in the case of LuAG:Ce^{3+}@SiO_2 PiG color converter.[43] The surface of the pristine LuAG:Ce^{3+} is smooth and clean (**Figure 10**a), and after coating the nano-sized (100–200 nm) SiO_2 particles aggregate on the surface of LuAG:Ce^{3+} (Figure 10b). EDS mapping of an individual LuAG:Ce^{3+}@SiO_2 particle displays the typical EDS signal of Lu and Si (Figure 10c,d). After the introduction of phosphor particles into glass, the uniform distribution of LuAG:Ce^{3+}@SiO_2 particles among the glass matrix can be observed (Figure 10e,f). There is no obvious interfacial reaction for the LuAG:Ce^{3+}@SiO_2 GC, while a transition area in grey scale (with a thickness of 0.5–1.5 μm) is found for the pristine LuAG:Ce^{3+} GC, which indicates the phosphor coating suppresses the phosphor-glass reaction (Figure 10g,h). The SiO_2 coating on one hand prevents oxidation of Ce^{3+} to Ce^{4+} and on the other hand retards interfacial reaction between the phosphor and the glass matrix. As expected, the fabricated $Lu_3Al_5O_{12}$:Ce^{3+}@SiO_2 GC exhibits ≈10% higher QE than that of pristine $Lu_3Al_5O_{12}$:Ce^{3+} GC. Remarkably, the optimized w-LED yields a high LE of 128 lm/W upon driven by 500 mA current.

Kim et al. found that the pore properties in GC have great impacts on LE and color quality of the GC-based w-LED.[44] In the experiments, a series of SiO_2-B_2O_3-ZnO glass frits were synthesized by adding different glass modifiers (Na_2O, Li_2O, La_2O_3, and WO_3), which were then blended and melted with YAG:Ce^{3+} at different sintering temperatures to gain various extents of glassy viscosity and then porosity. As the viscosity decreases, it is found the mean pore size and porosity increase due to pore coalescence

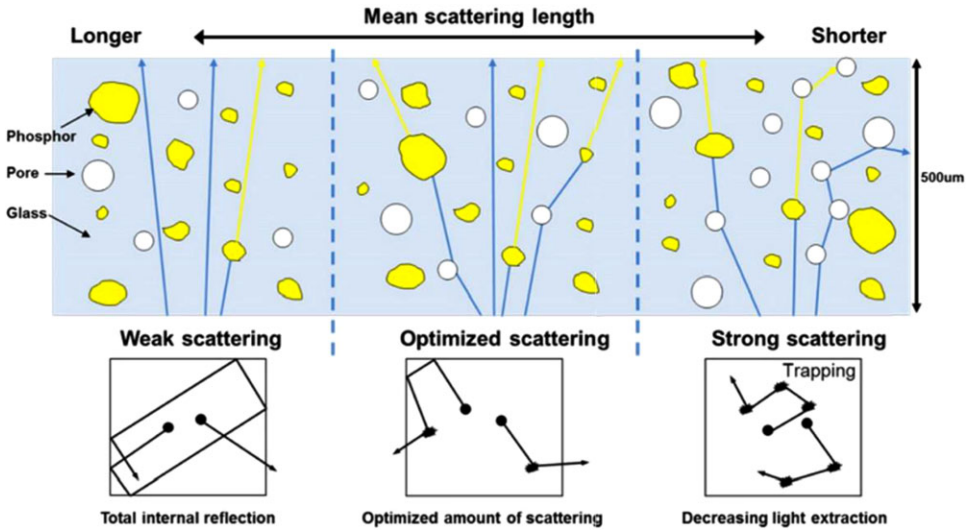

Figure 11. Schematical illustrations of three types of interaction between phosphor and blue light. Reproduced with permission.[44] Copyright 2015, American Optical Society.

and expansion, resulting in the change in scattering event. An interaction model of mean scattering length with scattering type based on the difference in pore properties is established (**Figure 11**), which explains the phenomenon that a higher LE is observed in the case of intermediate scattering length, due to the optimized interaction between pores and light. This model coincides well with the emission intensity data for the GCs. The effect of pore properties on CCT and CRI, as well as the relationship between the blue/yellow (B/Y) intensity ratio and the scattering type reveal that the CCT changes from cool white to warm white with increasing the pore size and porosity.

Yie et al. studied the influence of glass-phosphor mixing condition, i.e., phosphor size and content, on the micro-morphology and the optical properties of PiG color converter.[45] It reveals three main factors, i.e., 1) the cross-sectional area of phosphor particles, 2) the change in porosity during sintering process, and 3) the change in individual phosphor emission intensity, are responsible for the difference in luminous properties, such as, CCT, CRI, and transmittance. The first two factors influence the light scattered through the GC sample, as well as, the interaction between phosphor particles and blue LED light; whereas the third factor directly influences the emitted yellow light. It is confirmed that a desired color property of GC can be achieved simply by manipulating the phosphor size distribution.

Seo et al. took an in-depth look at the influence of refractive index of glass matrix on luminous performance of the GC-based w-LED.[46] It is found the glass modifiers, La_2O_3 and WO_3, creates more non-bridging oxygen with high polarizabilitiy in glass, which leads to an increase in refractive index, and thus the light extraction efficiency of w-LED package, due to the minimization of light loss by total internal reflection. Since more yellow light extracts from w-LED package, the emissive color evolves from cool to warm, and meanwhile CRI decreases.

Yoon et al. developed a novel gas pressure sintering method to prepare the fully dense PiG color converter.[47] In the experiment, 40 wt% amber Ca-α-SiAlON phosphor was co-sintered with SiO_2-B_2O_3-RO (R = Ba, Zn) base glass at 750 °C and then gas-pressured within GC at 710 °C for 30 min in 2000 kPa under N_2. As demonstrated in **Figure 12**a,b, the micro-pores with a size of around 10 μm are eliminated after the gas pressure sintering, which is demonstrated beneficial to producing good luminescent performance. The obtained Ca-α-SiAlON GC was then cut into a size of 1.2 mm × 1.2 mm and mounted on vertical LED chip. The GC thickness dependent EL spectra demonstrate the increased absorption of Eu^{2+} converting into orange emission due to the increased optical path. The internal QE of Ca-α-SiAlON GC reaches up to 74%. Upon 350 mA current driven, w-LED yields luminous flux of 88 lm. The reliability of the constructed amber w-LED is verified under a high-power operation current of 1 A and 85 °C/85%RH environmental condition. Evidently, the GC exhibits much better stability than its silicone counterpart with the luminous flux maintained up to 97% after 1000 h.

4. Material Systems

Aiming to obtain GC for w-LEDs, to date, many glass systems, including silicates, aluminosilicates, borates, borosilicates, phosphates, phosphosilicates, tellurites, boro-tellurites, antimonies, tin-phosphates, etc., are chosen as glass matrix to accommodate phosphor particles. Eu^{2+}, Ce^{3+}, Eu^{3+}, Mn^{2+}, Mn^{4+} activated aluminates, silicates, nitrides, fluorides, etc. as well as quantum dots are selected as phosphors. Table 3 collects a summary of the reported material systems and their corresponding luminescent behaviors.

4.1. GC for Blue-Excited Cool w-LEDs

As known, the major commercial w-LED is made of the InGaN blue-emitting chip and the YAG:Ce^{3+} yellow phosphor, yielding cool white light with correlated color temperature (CCT) >6000 K and color rendering index (CRI) <70. The fabrication of YAG:Ce^{3+} embedded GC, catering to the matured blue-excited

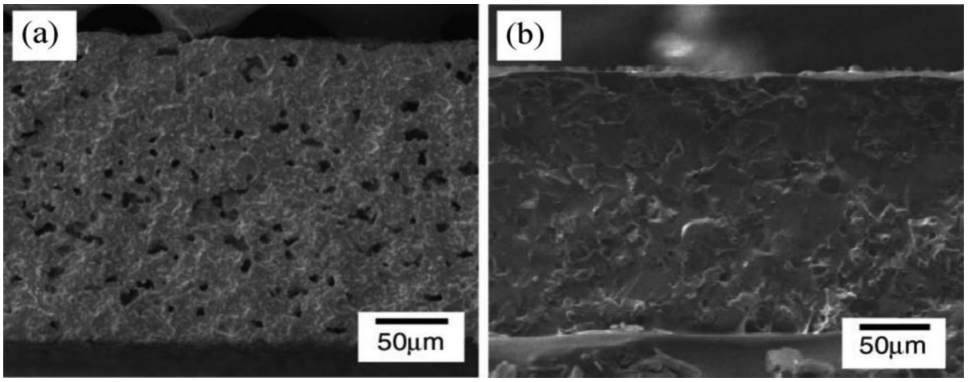

Figure 12. SEM images of the fractured surface of GCs embedded with 40 wt% of Ca-α-SiAlON a) without and b) with gass-pressure sintering. Reproduced with permission.[47] Copyright 2016, American Optical Society.

w-LED technology, has long-term been the focus of researcher's concern.

In 2005, Tanabe et al. first reported the YAG:Ce^{3+} GC by annealing the Ce-doped SiO_2-Al_2O_3-Y_2O_3-Li_2O precursor glass, which opens up a promising avenue to achieve long-lifetime high-power w-LEDs based on the all-inorganic color converter.[14,122–125] Glass crystallization occurs upon annealing the precursor glass at an appropriate temperature, turning the appearance color of glass from light brown to translucent yellow. SEM observation reveals that YAG:Ce^{3+} particles with the grain size of ≈20 μm are uniformly precipitated among the glass matrix. Upon blue LED excitation, the white light due to the mix of yellow and blue light is observed, demonstrating Ce^{3+} enters into the crystal lattice of YAG. QE of the YAG:Ce^{3+} GC, highly dependent on the annealing temperature of the precursor glass, is estimated to be ≈30%. It is thought that the contaminants from glass-matrix, such as Si^{4+} and Li^{+}, would incorporate into YAG crystals due to high annealing temperature of 1200–1500 °C, which serve as the fluorescence-quenching centers. YAG:Ce^{3+} GC exhibits a much better high-temperature/humidity resistance than the organic resin counterpart.

To avoid thermal damage to the luminescent performance of YAG:Ce^{3+}, in 2012, Chung et al. presented an innovative and cost-effective technique, i.e., the "PiG" approach, to synthesize the YAG:Ce^{3+} GC by co-sintering YAG:Ce^{3+} and Pb-free glass frits (SiO_2-B_2O_3-RO (R = Ba, Zn)) at low temperature of 750 °C for 30 min. [16] The obtained GC shows a certain transparency when polished into thickness of ≈250 μm (**Figure 13**a). SEM image and corresponding elemental analyses confirm good distribution of ≈10 μm sized YAG:Ce^{3+} within the glass matrix and negligible amount of interaction between the two phases (Figure 13b). By simply changing the glass to phosphor ratio and the thickness of GC, the chromaticity coordination can be adjusted easily (Figure 13c,d). The comparison made in thermal quenching behaviors between the GC and the phosphor-in-silicone (PiS) color converters demonstrated a much higher thermal stability in GC due to the robustness of glass. It is found that PL intensity in GC decreases only 7% at the temperature as high as 200 °C. In 2014, they reported the other kind of low-melting glass host (SiO_2-B_2O_3-ZnO-Al_2O_3-K_2O) with a much lower sintering temperature of 600 °C to accommodate the moisture-sensitive $SrGa_2S_4$:Eu^{2+}, demonstrating the thermal-/humidity-resistivity can be improved after incorporating $SrGa_2S_4$:Eu^{2+} into glass host.[63]

In fact, the proposal of using low-temperature co-sintering method to obtain YAG:Ce^{3+} GC can date back to 2010 by Cheng's group and Segawa's group. Cheng's results show the high-power w-LED based on 6 wt% of YAG:Ce^{3+}-doped glass exhibits 60% less lumen loss, 50% lower chromaticity shift, and 20% smaller transmittance loss than that with the YAG:Ce^{3+}-doped silicone, when treating the samples at 150 °C for 500 h.[15] In the following works, more systematic reliability tests, including 150 °C thermal aging for 1008 h, 85% RH/85 °C damp heat for 1008 h and −40 °C ≈ 125 °C thermal shock for 200 cycles, were conducted, confirming the feasibility of adapting GC as a phosphor-converted layer through providing a higher reliability and a better performance for high-end LED modules, particularly in the area where stability is highly required and in the environment where silicone can simply not stand for long.[126] However, they did not provide the detailed glass composition and the preparation procedure until the year of 2013.[40,127] In those works, the GC color converter was obtained by co-sintering the 4 wt% YAG:Ce^{3+} and the SiO_2-Na_2O-Al_2O_3-CaO glass frit at 700 °C, showing a moderate QE of ≈68%.[40] Segawa reported two kinds of glass systems, including R_2O-ZnO-B_2O_3 (R = Li, Na, K) and Na_2O-ZnO-TeO_2, to accommodate Ca-α-SiAlON:Eu^{2+}.[31] It is demonstrated that the tellurite glass is more suitable than borate glass as host due to the similar refractive index between glass and phosphor, as well as the lower melting temperature, despite Te atoms are more aggressive to phosphor particles.

Unlike the previous usage of silicate-based glass to co-sinter with YAG:Ce^{3+} at softening temperature (600-700 °C), in 2014, a new kind of low-melting glass, TeO_2-B_2O_3-Sb_2O_3-ZnO-Na_2O-La_2O_3-BaO, served as glass frit to co-sinter with YAG:Ce^{3+} at melting temperature (≈570 °C) (**Figure 14**), was developed in our lab.[8] This difference makes the preparation procedure of PiG color converter turn from tableting-sintering to re-melting. For tableting-sintering, the glass frit and phosphor powders could combine together at softening temperature, but there are a great number of trapped pores remained in the GC, which act as the scattering centers to reduce the luminescent performance of GC.[47] In contrast, treating the glass-phosphor composite at the melting temperature densifies GC. Benefiting from high reliability of the inorganic glass, the constructed GC-based w-LEDs

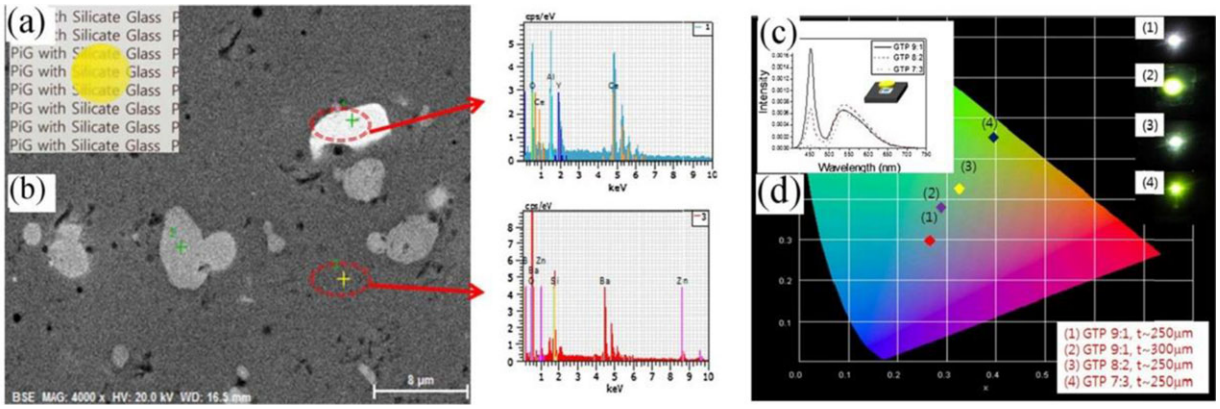

Figure 13. a) Photograph of GC plate. b) SEM along with EDS analysis on GC. c) EL spectrum and d) corresponding color coordination in CIE1931 diagram of GC-based w-LED by varying the glass to phosphor ratio. Reproduced with permission.[16] Copyright 2012, American Optical Society.

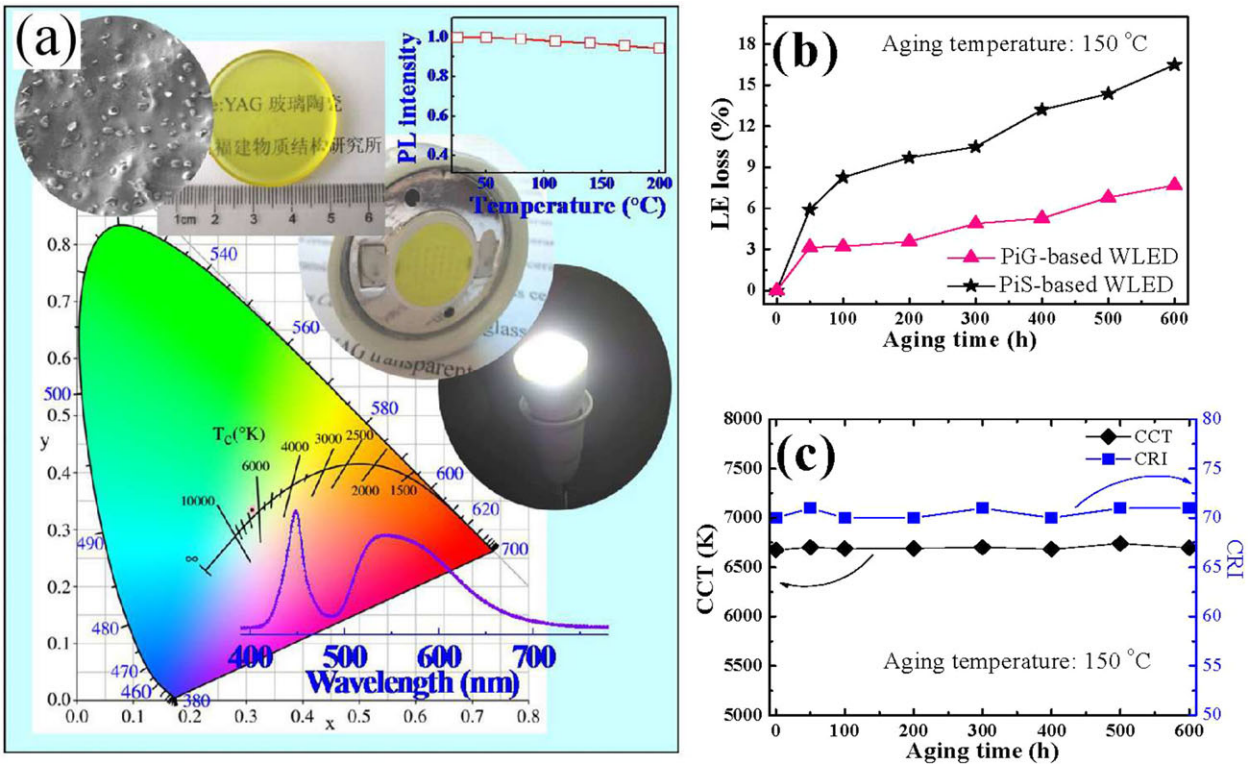

Figure 14. a) YAG:Ce^{3+} based GC and corresponding w-LEDs. Comparisons made for the b) LE loss and c) CCT/CRI between GC based w-LED and conventional silicone encapsulated w-LED. Reproduced with permission.[8] Copyright 2014, Wiley-VCH.

exhibit excellent heat/humidity resistance and thus gain longevity: only 7.6% LE loss is observed after aging at 150 °C for 600 h, much superior to that of the conventional PiS-based wLED (16.5%); and only 5.6% LE degradation is detected after immersing GC in the boiling water for 24 h. Besides the extended lifetime, the GC and the GC-based w-LEDs present excellent luminescent performance (QE = 93.5% for GC; LE = 124 lm/W at 350 mA for GC-based w-LED), thanking to the appropriate glass composition design by matching the refractive index between the glass matrix and the YAG:Ce^{3+} phosphors to reduce the light scattering loss at interface.

Depositing glass-phosphor composite on glass substrate in the form of film via screen-printing or tape-casting also attracts the researchers' interests. For example, Liu's group reported a well-defined and homogeneous film containing the SiO_2-B_2O_3-PbO glass powder and the YAG:Ce^{3+} phosphor, which is printed onto a glass substrate (**Figure 15**a).[35] YAG:Ce^{3+} in the size of ≈13 μm are found well distributed among the glass matrix without agglomeration (Figure 15b). A bright white light is observed when coupling the glass-phosphor composite with the commercial InGaN blue chip (Figure 15c,d). LE is found varying from 110.34 to 74.19 lm/W, when the input current is set from 40 to 500 mA

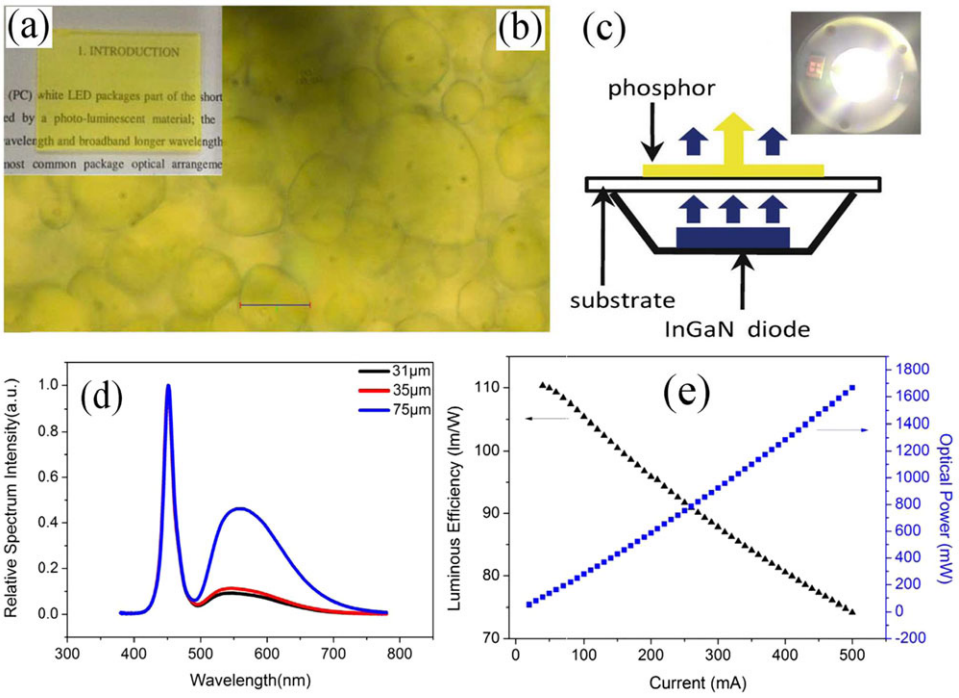

Figure 15. a) Appearance of the fabricated GC. b) Optical image of phosphor particles distribution on glass substrate. c) Schematic illustration of the fabricated GC-based w-LED and the luminescence photograph on state. d) GC thickness dependent EL spectrum of w-LED. e) Current dependency of LE and optical power for GC-based w-LED. Reproduced with permission.[35] Copyright 2013, American Optical Society.

(Figure 15e). Inspired by this work, many Pb-free glass systems for screen-printing, e.g., B_2O_3-SiO_2-M_2O-RO-Al_2O_3 (M = Na, K, Li; R = Zn, Ba),[102–105] TeO_2-B_2O_3-ZnO-Na_2O-Al_2O_3,[112] and P_2O_5-ZnO-B_2O_3-BaO,[113] have been developed recently.

4.2. GC for Blue-Excited Warm w-LEDs

According to the criterion of U.S. ENERGY STAR, YAG:Ce^{3+} GC cannot be applicable for indoor lightings due to the red spectral deficiency.[128] Aiming to overcome this shortcoming, there have been surges of researches attempting to introduce red components, such as the Eu^{2+}-activated nitride phosphors, the $Eu^{3+}/Mn^{2+}/Mn^{4+}$ emissive dopants, the Eu^{3+}/Mn^{4+} activated oxide phosphors, as well as the quantum dots, into the YAG: Ce^{3+} GC.

The commercialized $CaAlSiN_3$:Eu^{2+} (CASN:Eu^{2+}) nitride phosphor is usually regarded as the most appropriate red compensator for its high QE (>90%) and excellent thermal stability. Unfortunately, it easily undergoes chemical decomposition at high temperature, and/or thermal corrosion during glass-melting, i.e., serious reaction occurs between the glass constituents and the CASN:Eu^{2+} particles, making the GC turn dark. There are only very limited cases of success to incorporate CASN:Eu^{2+} into glass via the low-temperature co-sintering route. Chung's group first reported the control of chromaticity from cool to warm in the YAG:Ce^{3+}+CASN:Eu^{2+} embedded GC.[60] The low sintering temperature (550 °C) of SiO_2-Na_2O-RO (R = Zn, Ba) base glass enables the inclusion of CASN:Eu^{2+}. SEM image clearly shows both of the YAG:Ce^{3+} and CASN:Eu^{2+} particles with the sizes less than 10 μm well distribute within the glass matrix (**Figure 16**a). No reactions between the glass matrix and the yellow/red phosphors are found from their characteristic compositions clearly identified with EDS. By varying the weight ratio of glass to phosphor and that of YAG:Ce^{3+} to CASN:Eu^{2+}, the precise control of w-LED chromaticity can be easily achieved, following the Planckian locus very well (Figure 16b).

Most recently, Chung's group developed a brand new kind of glass system SiO_2-P_2O_5-ZnO-B_2O_3-R_2O (R = K and Na) as matrix for embedding YAG:Ce^{3+} and CASN:Eu^{2+} to fabricate the chromaticity-tunable w-LED.[67] There is no heavy metal element in the glass and the glass can be sintered at the temperature of merely 500 °C. Remarkably, CRI is ultra-high, even up to 93, after coupling GC with blue-chip to form w-LED.

Our group focused on the other kind of glass system SnF_2-SnO-P_2O_5 with glass melting temperature <400 °C, in the hope that CASN:Eu^{2+} can retain its original luminescent property at a lower temperature.[93] The use of this glass as matrix for GC-based w-LED was first proposed by Do's group, where the fabricated w-LED using YAG:Ce^{3+} GC as color converter yields cool white light with a LE of 118 lm/W, a CCT of 4275 K, a CRI of 68, and an external quantum efficiency (EQE) of 0.33 at an applied current of 350 mA.[9] In our work, it is found the warm white light can be realized with a LE of 90.71 lm/W (350 mA) and a CCT of 3554 K in the YAG:Ce^{3+}+CASN:Eu^{2+} GC-based w-LED, *viz*. good color quality and high luminous efficacy are simultaneously achieved.

Except the CASN:Eu^{2+} nitride, the other red phosphors, such as, Mn^{4+} or Eu^{3+} doped oxide, also seized the researchers'

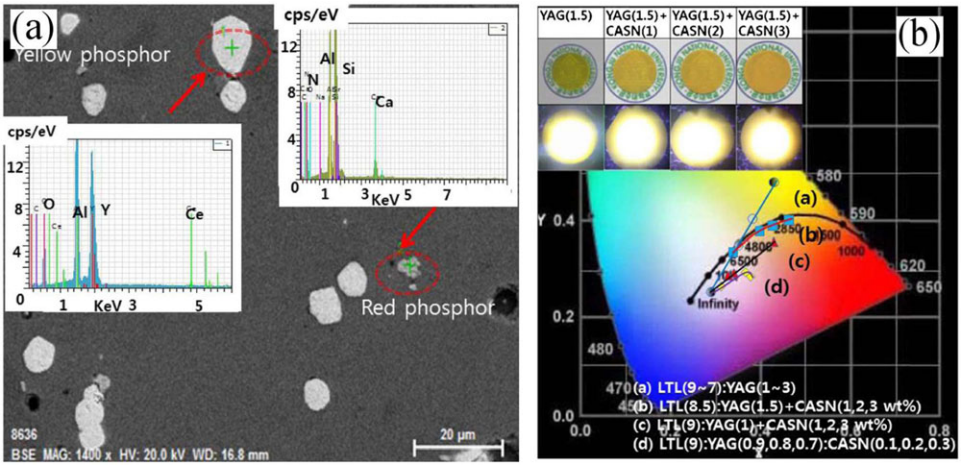

Figure 16. a) SEM image and EDS results of YAG:Ce^{3+} and CASN:Eu^{2+} embedded GC based on the SiO_2-Na_2O-RO (R = Zn, Ba) glass. b) Photographs and CIE coordinates of corresponding GCs with varying contents of YAG:Ce^{3+} and CASN:Eu^{2+} phosphors. Reproduced with permission.[60] Copyright 2013, American Optical Society.

attention and were attempted to introduce into glass host in accompany with YAG:Ce^{3+}. One typical example is the inclusion of $BaMgAl_{10-2x}O_{17}$:xMn^{4+},xMg^{2+} (BMA:Mn^{4+},Mg^{2+}) into the TeO_2-B_2O_3-Sb_2O_3-ZnO- Na_2O-La_2O_3-BaO glass (**Figure 17**a).[81] The unique structural feature of BMA, i.e., the alternative arrangement of Mn^{4+}-doped $MgAl_{10}O_{16}$/un-doped BaO layers in *z* direction, and that of Mn^{4+}-doped $[AlO_6]$/un-doped $[AlO_4]$ groups in *x*-*y* plane, favor efficient Mn^{4+} luminescence by reducing the non-radiative energy loss channels. BMA:Mn^{4+},Mg^{2+} embedded GC inherits spectral properties of the original powder. Thanks to the red supplement of Mn^{4+}, chromaticity parameters of YAG:Ce^{3+} GC-based w-LED can be well tuned with CCT decreasing from 6608 K to 3622 K, and CRI increasing from 68.4 to 86.0, meeting the requirement for indoor lightings. Likewise, $CaMg_2Al_{16}O_{27}$:Mn^{4+},[80] YAG:Mn^{4+},Mg^{2+},[89,90] $SrMgAl_{10}O_{17}$:Mn^{4+},Li^+ [[91]] red phosphors are also demonstrated possessing good ability to tune the spectral property of YAG:Ce^{3+} GC. The other interesting example is the partition of garnet-based $Li_6CaLa_2Sb_2O_{12}$:Eu^{3+} (LCLSO:Eu^{3+}) into glass host (Figure 17b).[85] LCLSO:Eu^{3+} exhibits highly efficient red luminescence in absence of the concentration quenching. The large Eu^{3+}-Eu^{3+} distance and the subsequent hampering of unwanted energy migration among them is believed responsible for this phenomenon. After fabricating into GC, the adverse energy transfer between Ce^{3+} and Eu^{3+} is efficiently suppressed, due to the spatial separation of Ce^{3+} in YAG lattice and Eu^{3+} in LCLSO lattice. As a consequence, QE of the GC reaches as high as 89.3%, and the constructed w-LED exhibits an optimal LE of 101 lm/W, a CCT of 5449 K and a CRI of 73.7 (Figure 17c). The other examples of introducing Eu^{3+} doped oxides into glass host include $La_2Ti_2O_7$:Eu^{3+} [[87]] and $La_{0.5}Na_{0.5}TiO_3$:Eu^{3+} perovskite.[88]

Spectral modification of YAG:Ce^{3+} GC by co-doping red-emissive rare-earth ions (Pr^{3+}, Eu^{3+}) or transition-metal ions (Mn^{2+}) has also been intensively investigated. Our group successfully introduced home-made YAG:Ce^{3+},Mn^{2+},Si^{4+} into TeO_2-B_2O_3-ZnO-Na_2O-Al_2O_3 glass matrix. [33] Thanking to the efficient energy transfer from Ce^{3+} to Mn^{2+}, the red emissive component in YAG:Ce^{3+} GC is greatly intensified (**Figure 18**a); correspondingly, the chromaticity of GC-based w-LED is readily tuned from cool to warm (Figure 18b). By further optimizing the thickness of GC plate, the chromaticity coordinate can be intentionally adjusted along the Planckian locus, locating in the eight quadrangles specified by American national standard (ANSI C78.377) for general lighting.[128] With increasing the Mn^{2+}/Si^{4+} content, LE declines monotonously from 105.9 to 39.6 lm/W, due to the decrease in yellowish green component of Ce^{3+}. The much improved thermal- and color-stabilities of GC-based warm w-LED than that of PiS-based one are demonstrated via an accelerated experiment through treating the samples at 150 °C for 1000 h.

Chung's group proposed a new "phosphor-in-fluorescent-glasses" (PiFG) strategy by doping red emissive ions into glass to tune color property of the YAG:Ce^{3+} GC.[59,67–69] The glass systems of PbO-B_2O_3-SiO_2 and Pb-free SiO_2-B_2O_3-RO (R = Ba, Zn) were employed. The influence of Eu^{3+}, Pr^{3+} or Mn^{2+} dopant on the luminescent performance of GC was carefully examined. It is found the introduction of red dopant shifts color coordinate and reduces color temperature of the YAG:Ce^{3+} GC-based w-LED; however, the red contribution is rather limited due to the following aspects: 1) the 4f-4f or 5d-5d absorption has low oscillator strength due to parity-forbidden nature; 2) the inherently limited conversion efficiency restricts the color adjustment role of theses ions; 3) the reabsorption of the YAG:Ce^{3+} radiative emission by the dopant reduces the overall emission intensity; and 4) the solubility limit hinders the further color adjustment due to concentration quenching. Chen et al. found that the spatial separation of Ce^{3+} and Eu^{3+} activators in GCs, where Ce^{3+} locates in the YAG crystalline phase while Eu^{3+} stays in the glass matrix, is advantageous to the realization of both intense yellow and red emissions, due to the suppress of adverse energy transfer between them (Figure 18c).[86] However, the obtained white light is not so warm with the CCT merely be 4541 K (Figure 18d).

The warm white light can also be achieved via the phosphor geometry configuration design based on multi-layered structure or patterned structure. In comparison with the conventional randomly mixed phosphor, such designs prevent serious reabsorption of yellow/green light emission by red phosphor and thus are

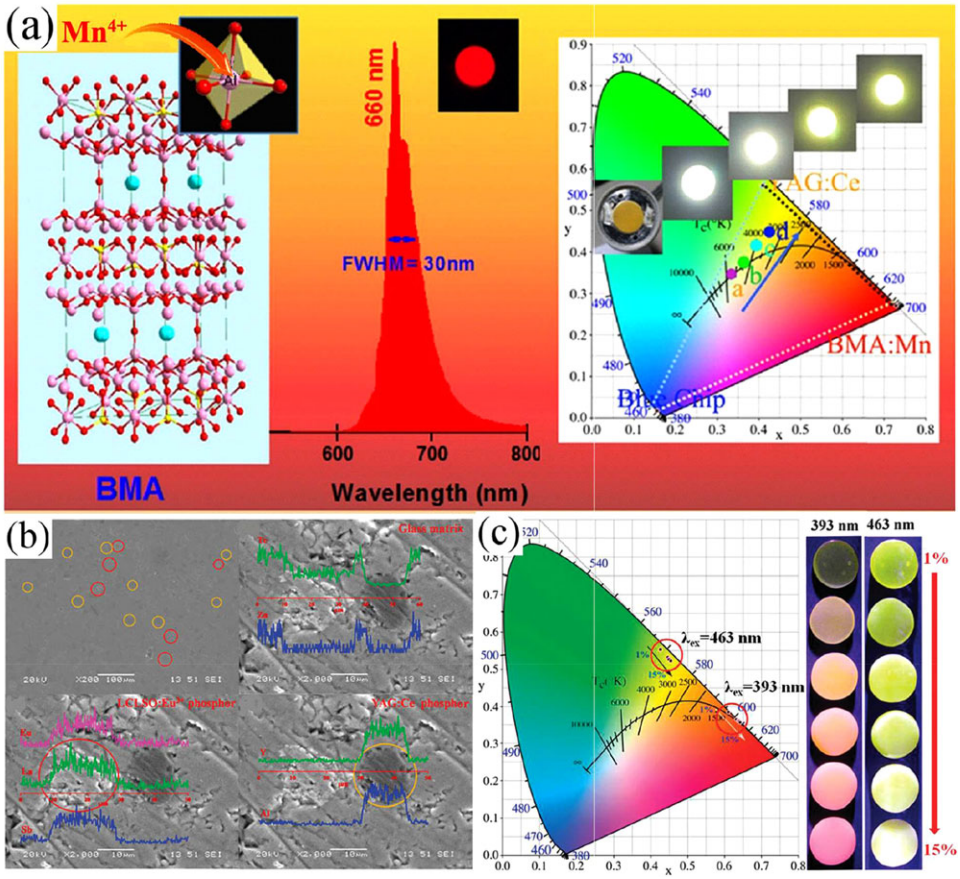

Figure 17. a) xMn^{4+},xMg^{2+}:BMA red phosphor, the corresponding GC, and GC based warm w-LEDs. Reproduced with permission.[81] Copyright 2016, American Chemical Society. b) the microstructure of GC embedded with LCLSO:Eu^{3+}. c) CIE color coordinates of the GCs with various LCLSO:Eu^{3+} contents (1-15 wt%) and a fixed Ce:YAG content (3 wt%). Reproduced with permission.[85] Copyright 2015, Royal Society of Chemistry.

beneficial to improving LE and color quality of the constructed w-LED.

Our group demonstrates a facile chromaticity tuning by depositing CASN:Eu^{2+} PiS on the YAG:Ce^{3+} GC via spin-coating (**Figure 19**a,b).[82] It is found that the stacking order influences EL performance of the constructed remote-type w-LED significantly. Placing the yellow layer close to chip die leads to a much higher LE, which is contrary to the result in the conformal-type w-LED. The used "scattered photon extraction" (SPE) structure for extracting backward-emitted photons (Figure 19c) is believed the main reason, since the backward-emitted photons lost in conformal-type w-LED would contribute to the total luminous flux in remote-type one, which results in the first layer close to chip die be a dominant layer. The optimized Y-GC/R-PiS based warm w-LED driven by 350 mA current yields a LE of 93.9 lm/W, a CCT of 3346 K, and a CRI of 77.3.

Im's group developed a new stacking design by mounting the $CuInS_2$/ZnS core-shell quantum dot embedded silica (QDES) film on GC (Figure 19d–h).[64] The film is made by dispersing QDES in the ETPTA resin. Remote phosphor configuration is used for reducing thermal damage to QD and providing smooth chromaticity variation/enough diffusing effect. It is proposed that the GC maintains a higher temperature gradient across it and thus blocks the thermal stress on QDES from the LED chip; moreover, GC withstands and protects ETPTA from the usual photo-induced damages on packaging materials. A comparative study was made on the EL stability of different configurations, where the YAG:Ce^{3+} GC plus Q-ETPTA film exhibits the most outstanding performance (Figure 19i).

Im's group also developed an innovative strategy by cutting and reassembling the red CASN:Eu^{2+} and the green LuAG:Ce^{3+} GCs as alternate quadrants to resolve the spectral overlapping problem.[62] The distinguishable emission bands from the component phosphors are clearly observed when using this phosphor geometrical design; while the green emission is merged into the broad band peaking in the red region when using the conventional phosphor mixing design, confirming the photon reabsorption can be greatly reduced in the former case. In the further work, they proposed a facile one-step fabrication technique to eliminate the interfacial layer between alternate quadrants and hence the leakage of light through this layer.[65] **Figure 20**a exhibits the digital photograph of the one-step fabricated GCs and their luminescent photographs on state. EL spectra obtained under an operating condition of 350 mA and 20 V demonstrates much higher emission intensity in GC via the one-step route (Figure 20b). CIE-1931 chromaticity coordinates of the constructed

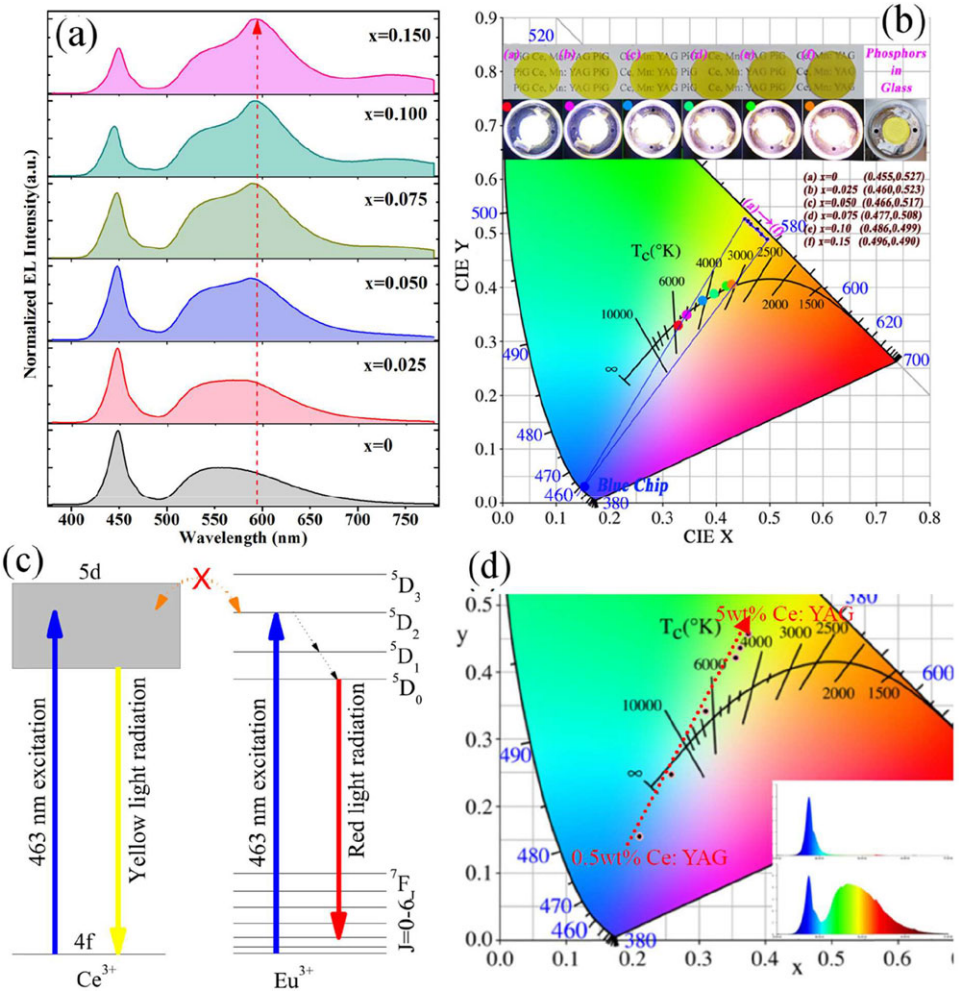

Figure 18. a) EL spectra of the YAG:0.06Ce^{3+},xMn^{2+},xSi^{4+} (x = 0-0.15) GC-based LED devices under 350 mA driving current. b) CIE coordinates of the YAG:0.06Ce^{3+},xMn^{2+},xSi^{4+} GCs and the corresponding LEDs; insets are digital photographs of GCs and GC-based LEDs in operation. Reproduced with permission.[33] Copyright 2015, Royal Society of Chemistry. c) Schematic energy level diagrams of Ce^{3+} and Eu^{3+}, showing the cutoff of adverse energy transfer between Ce^{3+} and Eu^{3+} in GC. d) CIE color coordinates of the GC-based LEDs with various Ce: YAG contents (0.5-5 wt%) and a fixed Eu^{3+} content (1 mol%) in GCs. Reproduced with permission.[86] Copyright 2015, Wiley-VCH.

warm w-LED (CCT close to 3000 K) follow along the Planckian locus well (Figure 20c).

Inspired by Im's work, Chen's group prepared the patterned GCs with sector piece and concentric ring phosphor geometries using the screen-printing technique (Figure 20d,e).[102] Diverse light colors emit from the different parts of GCs at low current, since the yellow and red phosphor parts are separately excited by the blue LEDs (Figure 20f,h). The bright white light can be observed at high current (Figure 20g,i). Experimental results indicate that LED modules packaged by the patterned GCs yield a moderate LE (40–50 lm/W) with a CCT of 3700–4400 K.

4.3. GC for UV-Excited w-LEDs

W-LED based on the "UV chip + red, green and blue (RGB) phosphors" design also receives great interests for the benefits of high CRI, wide color gamut and stable light color output at different driving currents. Encasing RGB phosphors into glass matrix can not only improve the durability of phosphors, but also may overcome the problem of UV light leakage, since glass has strong absorption ability for UV light.

Aiming to obtain white light, RGB components should be finely tuned to balance their relative colormetric ratios. Our group proposed a "dopant isolation" strategy to achieve this goal by isolating different active ions into different crystals in GC.[50] The spatial isolation of different activators suppresses the energy transfer between them, allowing an accurate color manipulation. As shown in **Figure 21**a, two types of nanocrystals, *i.e.*, 20–30 nm sized β-YF_3 and 4–6 nm sized γ-Ga_2O_3 coexist in the glass matrix. Owing to the difference in ionic affinity, Tm^{3+} and Mn^{2+} were selectively partitioned into β-YF_3 and γ-Ga_2O_3 nanophases, respectively (Figure 21b), resulting in suppression of the adverse energy transfer between Tm^{3+} and Mn^{2+} that occurs in glass matrix (Figure 21c). Evidently, upon 360 nm excitation, the emissive color of GC can be facilely tuned from blue, green, yellow, red

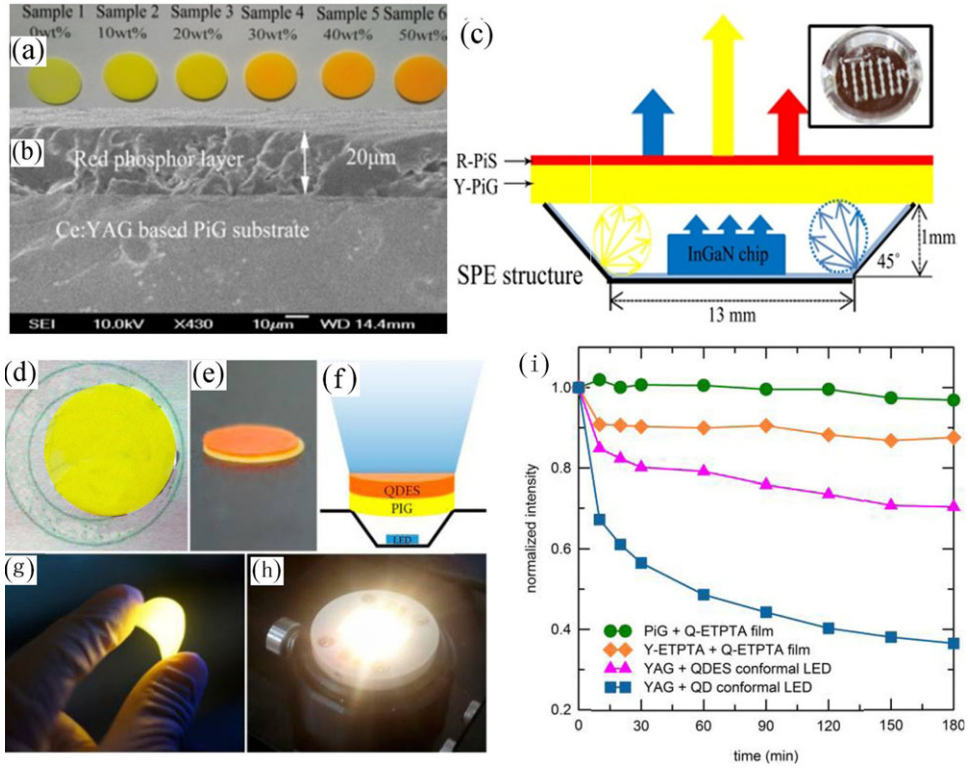

Figure 19. a) Photographs of the CASN: Eu^{2+}-PiS coated GC. b) SEM photograph of the cross-sectional sample. c) Schematic illustration of the fabricated remote-type w-LED. Reproduced with permission.[82] Copyright 2015, Elsevier. d) Photograph of a kind of YAG:Ce^{3+} GC. e) Q-ETPTA film stacked on GC. f) Schematic diagram of the WLED. g) Photograph of Q-ETPTA film under UV illumination. h) WLED under operation. i). EL stability test. Reproduced with permission.[64] Copyright 2014, American Chemical Society.

and white, just by varying the dopant species and concentration (Figure 21d).

Wang's group prepared a kind of chromaticity-tunable GC by dispersing $Ca_9Gd(PO_4)_7$:Eu^{2+},Mn^{2+} phosphor into SiO_2-Al_2O_3-B_2O_3-ZnO-BaO glass system, using the low-temperature co-sintering method.[75] GC inherits the color tunability of $Ca_9Gd(PO_4)_7$:Eu^{2+},Mn^{2+} phosphor. The optimized GC exhibits QE of 26.2% and excellent heat/humidity-resistance. Proof-of-concept warm w-LEDs by combining GC with near-ultraviolet chip-on-board exhibit good chromaticity performance (**Figure 22**a). Lei's group introduced the commercial $Sr_4Al_{14}O_{25}$:Eu^{2+} cyan phosphor into SiO_2-Al_2O_3-Na_2CO_3-CaO-Eu_2O_3 glass based on the aforementioned PiFG strategy.[72] Eu^{3+} doped glass frit exhibits the intense red emission under UV light (Figure 22b,c). By adjusting the mass ratios of $Sr_4Al_{14}O_{25}$:Eu^{2+} phosphor to glass frit, a series of multicolor GCs are obtained, exhibiting moderate QE of 52.3% and good resistance to harsh conditions. The corresponding GC encapsulated high-power LED devices are fabricated, showing several types of warm-white-emitting (Figure 22d,e).

4.4. GC for AC Driven w-LEDs

AC-LED, namely, a LED device driven directly by alternative current, has received constant industrial interests, owing to the tremendous merits of not only lower price (thanking to the reduced redundant electronic components), but also higher energy utilization efficiency, more compacted volume, and longer service life, in comparison with the DC-LED counterpart. However, a dimming time of 5–20 ms is unavoidable in every AC cycle, resulting in flicker effect. One promising route to compensate the flicker is utilization of afterglow luminescence in the persistent phosphors, as proposed by Liu et al.[129] Furthermore, the introduction of persistent phosphor into inorganic glass matrix endows AC-LED more reliability, hopefully expanding its application towards "high-power".

Our group successfully prepared a kind of persistent GC for AC-LED application by incorporating $Gd_3Al_2Ga_3O_{12}$:Ce^{3+} (GdAGG:Ce^{3+}) persistent phosphor into B_2O_3-TeO_2-ZnO-Na_2O-La_2O_3-BaO glass matrix.[83] Ga plays a key role in engineering the host bandgap, allowing the electrons' delocalization to conduction band under blue-light excitation and thus facilitating electrons' storage at the traps to achieve afterglow luminescence. SEM analyses demonstrate the size of GdAGG in the glass matrix ranged from 0.5 μm to 20 μm, similar to that of the GdAGG powders, indicating the glass-melting procedure influence the GdAGG microstructure insignificantly (**Figure 23**a,b). EDS line scan shown in Figure 23c confirms the chemical composition of the embedded GdAGG. Upon charging by 460 nm blue light, GdAGG:Ce^{3+} GC shows an average persistent lifetime of 115 ms in the millisecond time window, indicating its potential to compensate the AC time gap (Figure 23d). A remote-type AC-LED

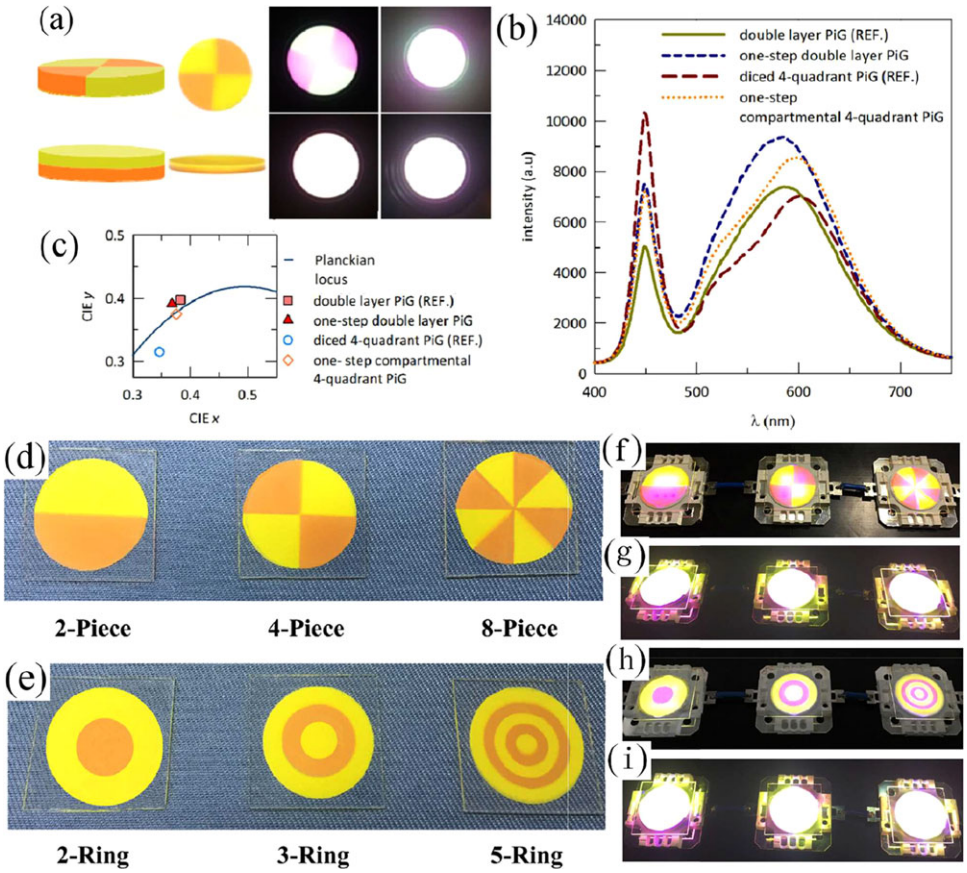

Figure 20. a) Digital photograph of the one-step fabricated GCs and their luminescent photographs on state. b) Corresponding EL spectra obtained under 350 mA and 20 V. c) CIE-1931 chromaticity coordinates of the constructed warm w-LED. Reproduced with permission.[65] Copyright 2015, American Optical Society. The prepared patterned GCs with d) the sector piece and e) the concentric ring phosphor geometries. f–i) Corresponding GC-based warm w-LEDs. Reproduced with permission.[102] Copyright 2016, Elsevier.

device based on the GC is constructed, which is then connected to an AC bridge circuit. It is found the flicker effect reduces from 100% to 69%, thanking to the compensation from the afterglow luminescence of GdAGG:Ce^{3+}.

4.5. GC for w-LD

Different from LED, the burgeoning laser diode (LD) doesn't produce "efficiency droop" mainly induced by the electron-hole Auger recombination at high driven current.[130] Moreover, LD shows the advantages of high efficiency, large luminous flux and small etendue, representing a new progress direction in the field of high-power solid-state lighting. However, w-LD exhibits a restricted service lifetime due to the serious heating effect from the high-energy laser irradiation. Aiming to overcome this deficiency, Zhang et al. attempted to adopt a robust YAG:Ce^{3+} GC as color converter.[76] Using a 488 nm confocal laser scanning microscope (CLSM), the surface fluorescence distribution of YAG:Ce^{3+} GC can be clearly observed (**Figure 24**a,b). 3D reconstruction images demonstrate the homogeneous spatial distribution of phosphor particles in the sample (Figure 24c). CL emission spectra of different points (1-10) on YAG:Ce^{3+} particle show a dominating band centered at 550 nm and a weak shoulder peaking at 350 nm (Figure 24d,e). This weak UV emission is attributed to the presence of Y^{3+}_{Al} anti-site defects, indicating that the YAG phosphor particles are intact as the powder. The prototype of modular w-LDs in Figure 24h is fabricated by combining 5 wt% YAG GC and blue LD, yielding bright white light in operation (Figure 24i). The emission spectrum consists of the line-emitting peak at ≈445 nm derived from blue LD and the yellow-emitting band from YAG:Ce^{3+} GC, with a color coordinate of (0.329, 0.333), a CCT of 5649 K, and a LE of 110 lm/W.

Xie's group also developed a kind of GC for w-LDs by incorporating β-Sialon:Eu^{2+} or CASN:Eu^{2+} into ZnO-B_2O_3-BaO-Al_2O_3 glass.[73,74] β-Sialon:Eu^{2+} GC shows a linear relationship between the luminous flux and the incident laser power when the blue laser flux density was below 0.7 W/mm^2.

4.6. GC for Backlight Display

The rapid development of liquid crystal display (LCD) technology has driven updating of backlight source from the cold cathode fluorescent lamps (CCFL) to the w-LEDs, for the merits of

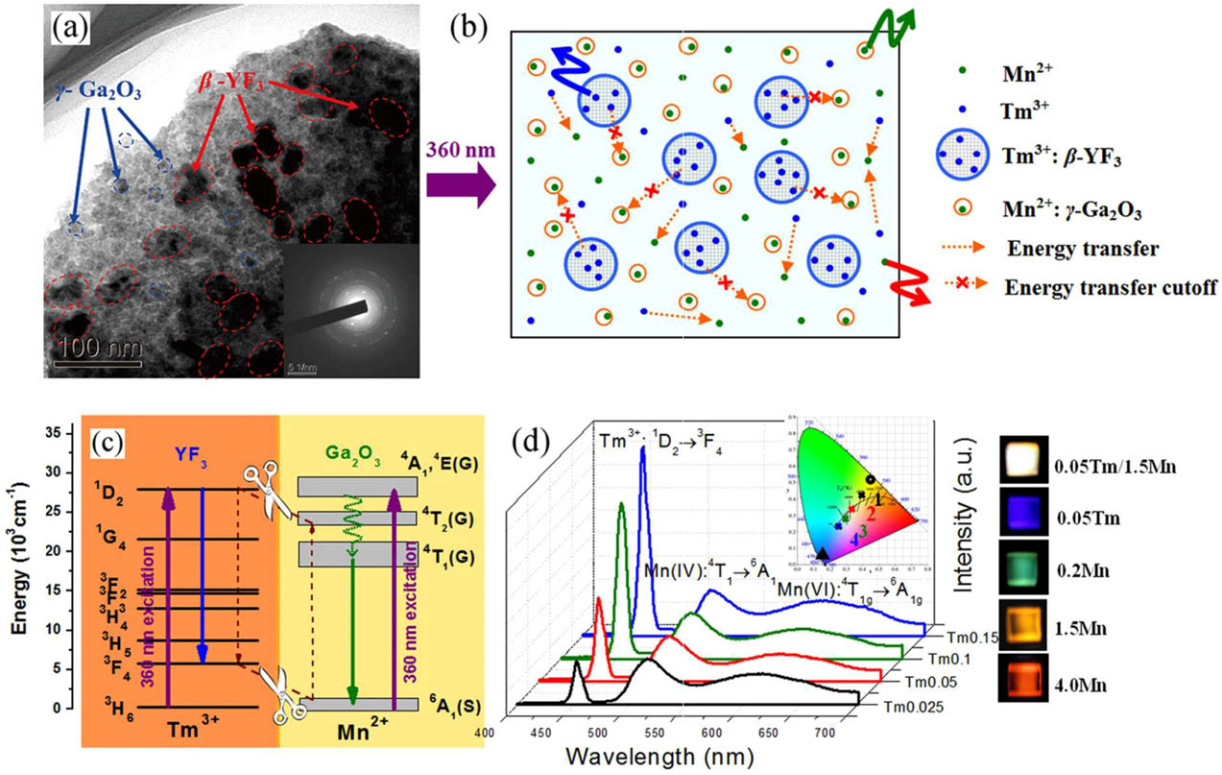

Figure 21. a) TEM micrograph of glass ceramic containing γ-Ga_2O_3 and β-YF_3 nanocrystals. b) A sketch shows the distribution and luminescent behaviors of Tm^{3+} and Mn^{2+} ions in GC. c) Schematic energy level diagram of Tm^{3+} and Mn^{2+} ions showing the energy transfer cutoff when they are partitioned into distinct nanophases. d) Photoluminescence spectra of x mol% Tm^{3+}/1.5 mol% Mn^{2+} (x = 0.025 ≈ 0.15) dual-doped GC under 360 nm excitation, inset is the CIE 1931 coordinate diagram showing chromaticity points of the corresponding samples. Reproduced with permission.[50] Copyright 2013, Royal Society of Chemistry.

high brightness, small volume, low power consumption, and mercury-free.[131,132] Aiming to faithfully reproduce all kinds of the natural colors, the color gamut of LCD, defined as the percentage of NTSC in CIE color space, should be as wide as possible, which requires narrowband emission and high efficiency in color converter.[133] The well-known phosphor candidates for backlight display include β-Sialon:Eu^{2+}, Mn^{4+}-activated fluorides, and halide perovskite QDs. They exhibit admirable spectral properties, however, suffer from the thermal or moisture-induced degradation under long-term use. Undoubtedly, introducing these phosphors into all-inorganic glass matrix to form GC can greatly improve their physical/chemical stability. Recently, β-Sialon:Eu^{2+} or perovskite QDs embedded GCs, exhibiting narrow full-width at half-maximum (FWHM), have been announced[73,134,135]; unfortunately their applications for backlight display have not received sufficient attentions yet. There should be more work to be done on this topic.

5. GC-Based w-LED Package Optimization

Aiming to achieve desirable optical and chromatic performance in high power w-LEDs, the adequate design of w-LED packaging is unquestionably critical.

5.1. Optical Model for GC-Based w-LED Package

Chen et al. established a precise model for GC layers to accurately predict the optical and chromatic performance of the GC-based w-LEDs.[136] 3D ray-tracing simulations are performed by *LightTools* software, with all the optical parameters for modeling derived from the measurement. In the procedure, the light scattering and trapping events are considered. The simulated emission spectrum and chromaticity coordinates of w-LED coincide with those of the measured one: the chromaticity deviation between the simulation and experimental measurement is within 0.012, and the CCT deviation within 184 K, which demonstrates good reliability of the simulation model.

5.2. W-LED Package Optimization by Constructing the GRIN Structure

As known, the total reflection and Fresnel reflection exist between the two mediums with different refractive indices. This issue is of great importance in w-LED package, since the unextracted photons reflecting back into LED chip converts to waste heat and finally rises the working temperature of chip die. Yang et al. proposed fabrication of GCs with gradient refractive index (GRIN) in different layers to solve this problem.[137] The

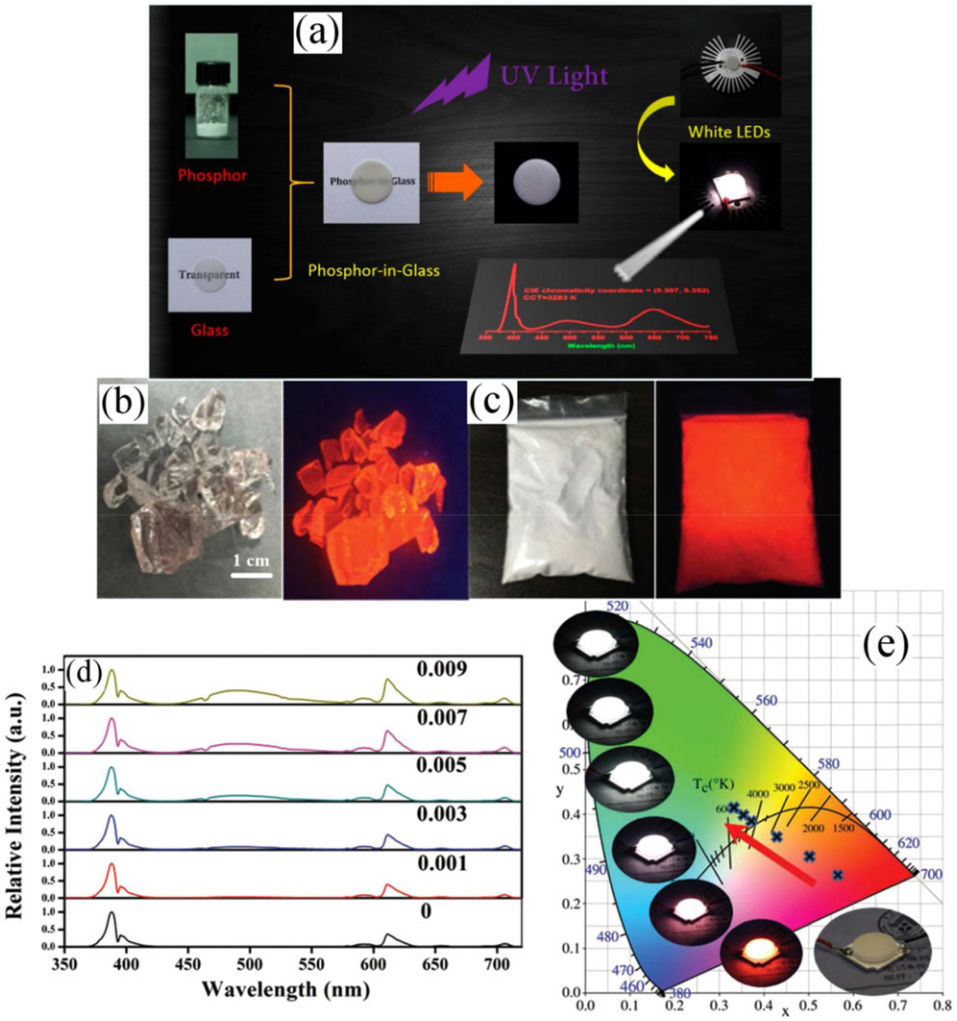

Figure 22. a) Preparation and performance of the $Ca_9Gd(PO_4)_7:Eu^{2+},Mn^{2+}$ embedded GC and corresponding GC-based warm w-LED. Reproduced with permission.[75] Copyright 2015, American Chemical Society. b,c) Eu^{3+} doped SiO_2-Al_2O_3-Na_2CO_3-CaO glass frit before/after grinding in daylight and under 365 nm UV lamp. d) EL spectra of warm w-LEDs constructed by coupling xEu^{3+} doped GC (x = 0-0.009) with UV chip. Reproduced with permission.[72] Copyright 2017, Wiley-VCH.

gradually decreased refractive index from chip to air allows more photons to be extracted, contributing to the luminous flux of w-LED (**Figure 25**a,b). The optical simulation results show the light extraction efficiency can be enhanced by >50%. Zhuo *et al.* fabricated the multilayer GRIN structure in YAG:Ce^{3+} GC by screen-printing.[113] The refractive index of the used P_2O_5-ZnO-B_2O_3-BaO (PZBB) glass can be tuned from 1.42 to 1.58 by increasing the molar ratio of BaO to ZnO. GRIN structure can be clearly observed in the surface topography (Figure 25c). In comparison with that of the conventional structure, the transmittance of GRIN structure increases by 91.33%, and the LE increases by > 28.87% (Figure 25d).

5.3. W-LED Package Optimization by Geometrical Design

Utilization of the layered or the patterned structure to resolve the issue of photon reabsorption in GC embedded with two or more kinds of phosphors had been intensively investigated by Im's, Chen's and Lee's groups.[62,65,102,110,111] The typical examples are presented in Section 4.2, which exhibits a much improved LE in GC by using these elaborate and smart geometrical designs.

5.4. Angular Color Uniformity (ACU) Optimization

Angular color uniformity (ACU) is an important parameter in practical application, determining whether or not the lighting source is comfortable to human eyes. It is known that the yellow ring phenomenon usually appears at the perimeter of the single-layer GC based w-LED, since the ratio of yellow to blue light is different in different parts of GC, leading to poor color uniformity. Wang et al. devoted themselves to improving ACU of the luminescent GC via multilayer screen-printing in a conical shape (**Figure 26**a,b).[97] As shown in Figure 26c, the deviation of CCT from −80° to 80° for the three-layer structure is merely 171 K,

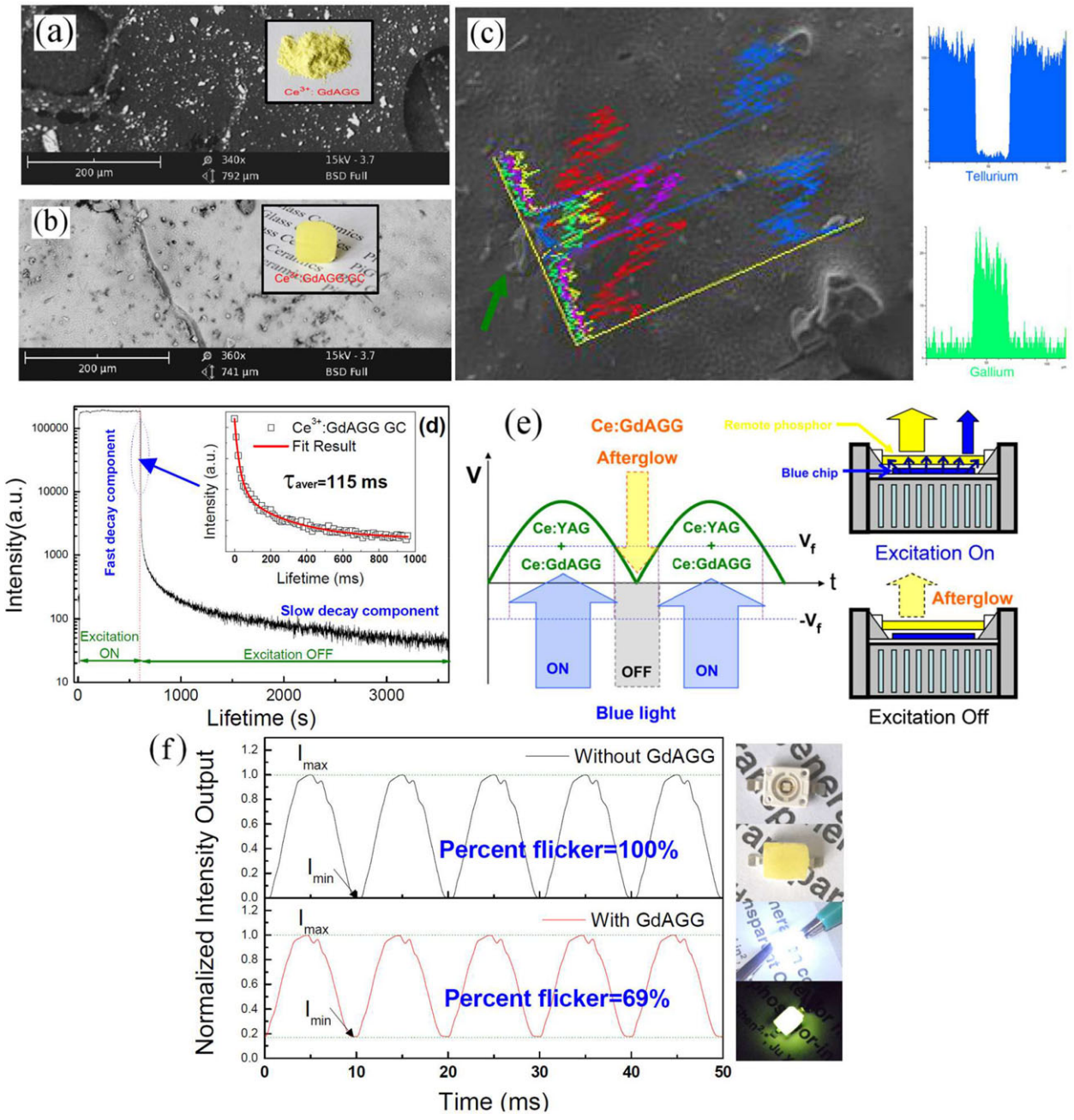

Figure 23. a,b) SEM images of the GdAGG powder and the fabricated GC containing 10% GdAGG; insets in (a) and (b) show photographs of the corresponding samples. c) EDS line scan curves showing Te, Ga, and O element profiles across the GC sample. d) Afterglow luminescence decay curve of Ce^{3+}: GdAGG GC; inset in (d) shows the initial 1s decay at a step of 10 ms after the stoppage of excitation source. e) The proposed scheme of applying persistent Ce^{3+}: GdAGG GC to AC-LED device with a bridge circuit design. f) Luminescence intensity variations of the labeled LED devices driven in AC periodic cycles. Reproduced with permission.[83] Copyright 2014, American Chemical Society.

which is much lower than those in the one- or two-layer structure, demonstrating the three-layer cone-shaped structure is greatly beneficial to improving ACU. This ACU performance enhancement is mainly attributed to the optimized multilayer geometry which facilitates the blue light escaping around the thinner peripheral region and impedes blue light escaping at the thicker center region; meanwhile, the converted yellow light emission is reduced around the peripheral and enhanced at the center due to the variation of the blue light absorption and conversion.

Kim et al. studied ACU of the 4-segmented GC, revealing an angular dependence of the color distribution, particularly significant for the blue and green components at a polar angle of 30° (**Figure 27**a–d).[65] Aiming to solve this problem, Peng et al. proposed usage of the microstructured glass plate in a

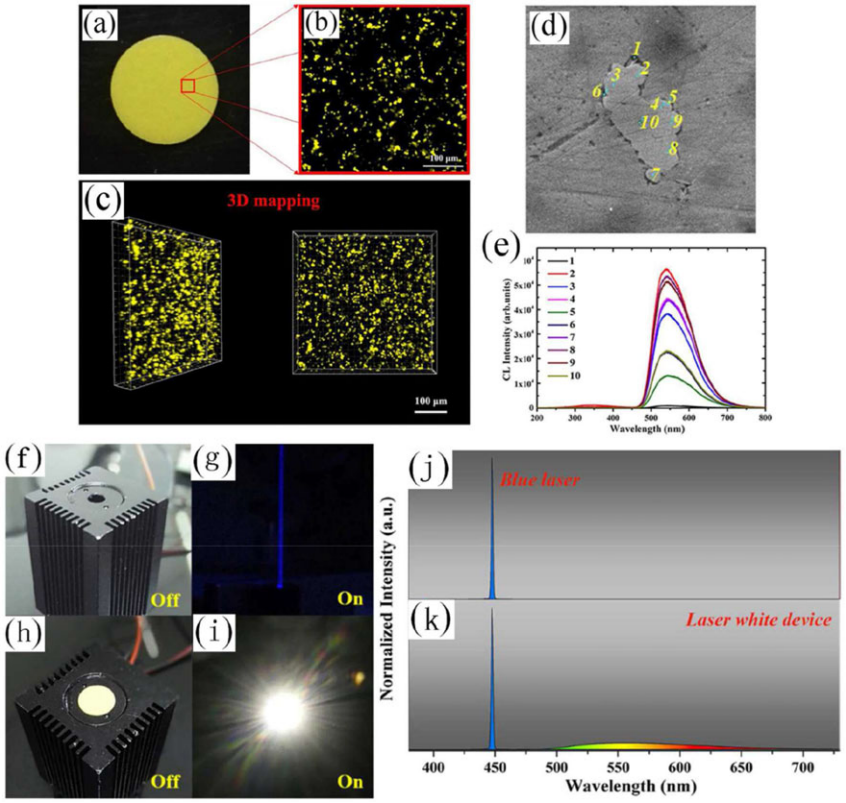

Figure 24. a) Photograph of 3 wt% YAG-GC sample. b) Surface fluorescence distribution image and c) 3D reconstruction images of 3 wt% YAG-GC sample. d) SEM and e) the point CL spectra of 3 wt% YAG-GC sample in single particle. Photographs of f,g) blue LDs and h,i) prototype white LDs combining blue LDs and 5 wt% YAG-GC out operation and in operation, respectively; Normalized EL spectra of j) blue LDs and k) prototype white LDs. Reproduced with permission.[76] Copyright 2017, American Chemical Society.

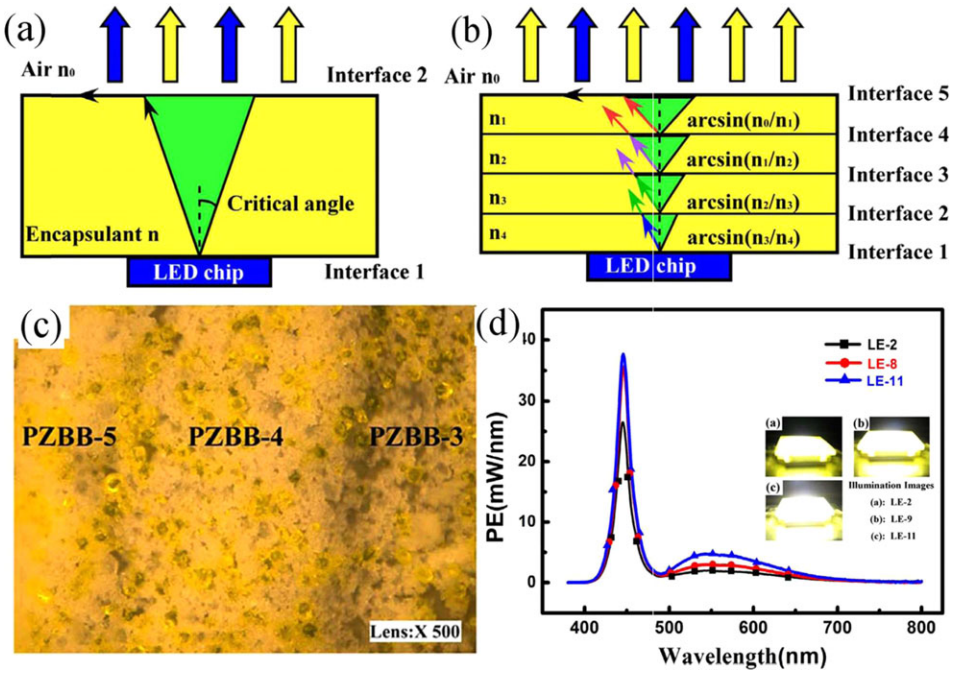

Figure 25. Schematical illustrations of the total reflection at interface between the LED chip and the encapsulant materials in a) conventional LED package and b) GRIN-structured LED package. c) GRIN structure images of YAG:Ce GC with three layers. d) Power spectra of emitting lights in different GRIN structures. Reproduced with permission.[113] Copyright 2017, Elsevier.

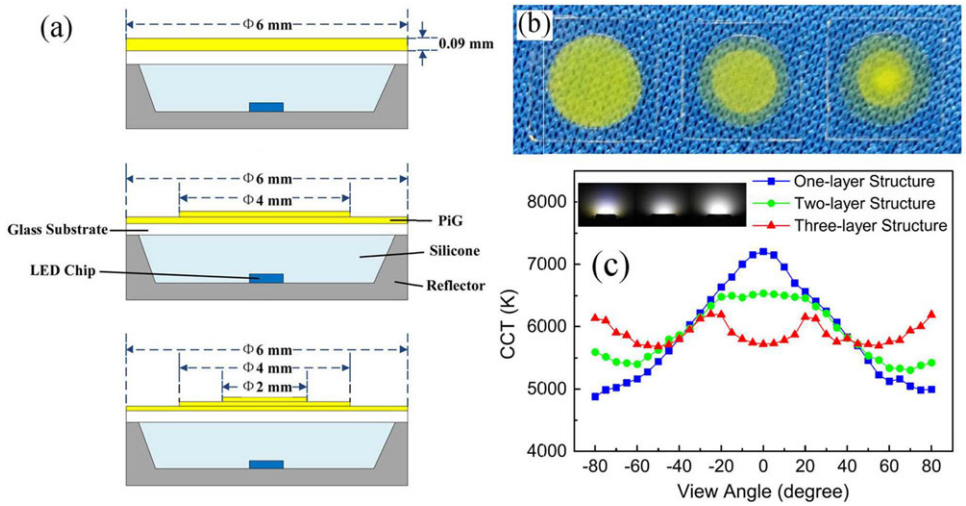

Figure 26. a) Schematic diagrams of the GC-based w-LED packaging models with different coating layers. b) Photograph of three types of GC in different layers. c) Angular color distributions of w-LEDs with one-layer, two-layer, and three-layer cone-shaped layer (CCT = ≈6000 K); the insets are the illumination patterns of GC-based w-LEDs in operation Reproduced with permission.[97] Copyright 2014, American Optical Society.

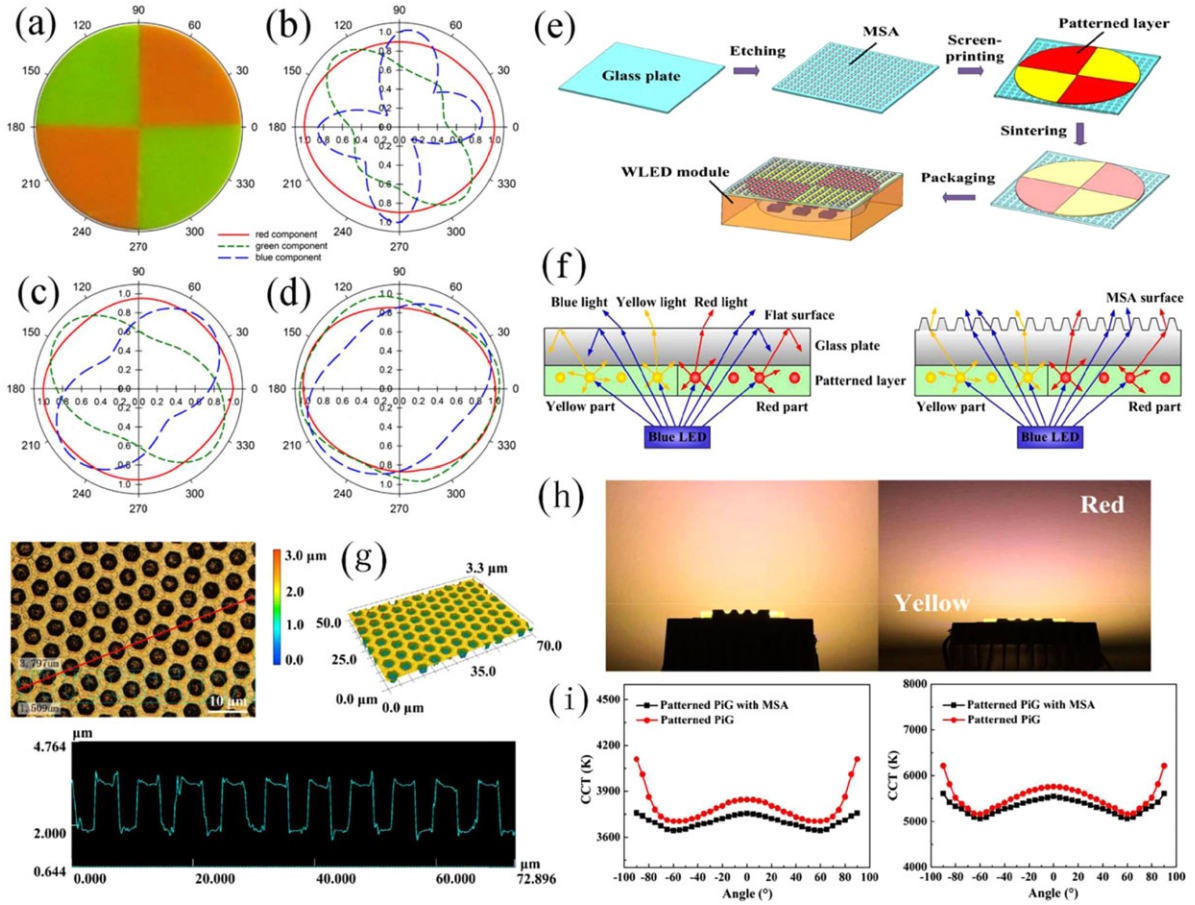

Figure 27. a) Digital photograph of the 4-segmented GC with labeled azimuthal angles. Polar plots of the relative intensities of red, green, and blue component colors at polar angles of b) 30°, c) 45°, and d) 60°. Reproduced with permission.[65] Copyright 2016, American Optical Society. e) Schematic illustration of the preparation process of w-LED packaged by patterned GC with MSA. f) Schematic illustration of light transmission in patterned PiG and patterned PiG with MSA. g) Laser scanning confocal microscopy pictures of MSA on the surface of glass plate. h) W-LED on state and i) angular color distribution of w-LED in the presence/absence of MSA. Reproduced with permission.[104] Copyright 2017, American Optical Society.

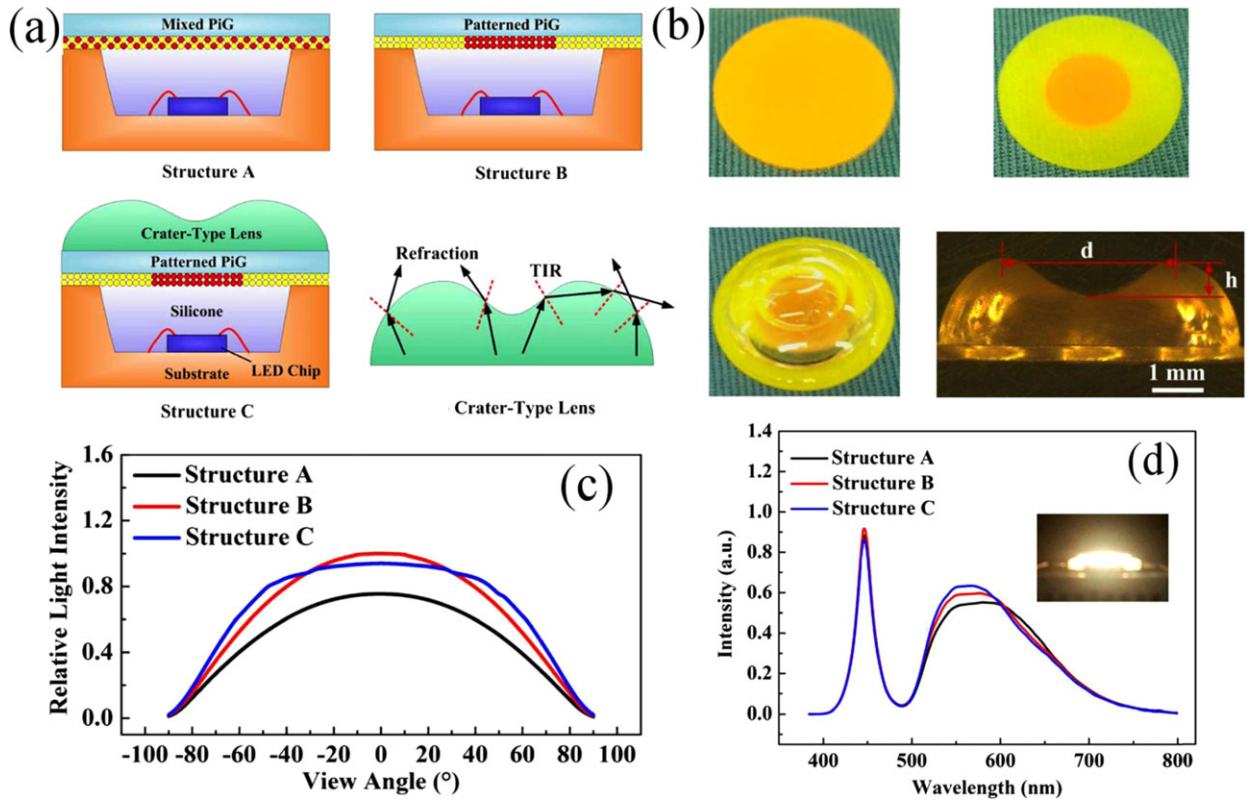

Figure 28. a) Schematic illustration and b) digital photograph of mixed structure, patterned structure, patterned structure with crater-type lens, and crater-type lens. c) Light intensity distribution and d) EL spectra of GC-based LEDs packaged by the three structures. Reproduced with permission.[106] Copyright 2016, American Optical Society.

microstructure array (MSA) (Figure 27e). [104] MSA scatters emission light over a large region, ensuring uniform CCT distribution and reduction in total internal reflection (Figure 27f). MSA is etched on the top surface of base-glass plate by an inductively coupled plasma etching. The diameter, height and space of the periodic inverted truncated cone array are optimized to 5 μm, 2.6 μm, and 2 μm, respectively (Figure 27g). Apparently, the w-LED using MSA on state eliminates the diverse color occurred in the patterned GC w-LED (Figure 27h). The angular color distribution measurements confirm a much lower CCT deviation in the w-LEDs using MSA (Figure 27i).

5.6. Secondary Optical Design

The secondary optical design is widely applied to the w-LED package to gain better photometric and chromaticity performance. The previously mentioned MSA belongs to this design, which not only improves the ACU, but also increases LE of the GC-based w-LED by 12.5%, due to the enlarged critical angle for allowing more photons to escape from the flat surface of glass plate.[104] Similar results were found in their related works of using the textured base-glass.[138,139] Peng et al. also proposed a new combined structure based on a ring-patterned GC with a crater-type lens (**Figure 28**a,b).[106] The optical performance in three types of the w-LEDs, *i.e.*, mixed structure, patterned structure, and patterned structure with a crater-type lens, were measured and compared with each other. Obviously, the light intensity distribution of structures A and B are both close to the Lambert distribution, while the light intensity distribution in structure C has a little alternation, since the emissions are redirected to large view angles by the crater-type lens (Figure 28c). EL spectral analyses (Figure 28d) reveal the crater-type lens with a cambered interface can decrease the TIR loss to some extent, resulting in a much higher LE (increased by 19.3% and 10.7%, respectively, in comparison with Structures A and B).

5.7. Thermal Management

High power condition produces enormous amount of the heat from chip, which damages the luminescent property of phosphor: firstly, QE reduces due to the increased probability of non-radiative phonon relaxation; secondly, color deviation occurs in multi-phosphors for the different thermal quenching behaviors. Thanking to good thermal conductivity of the glass matrix (≈1 W/mK), GC served as the color converter is believed a promising solution to high-power application. However, the accumulated heat in GC still exerts negative effect on the luminescent performance of the embedded phosphor particles, especially

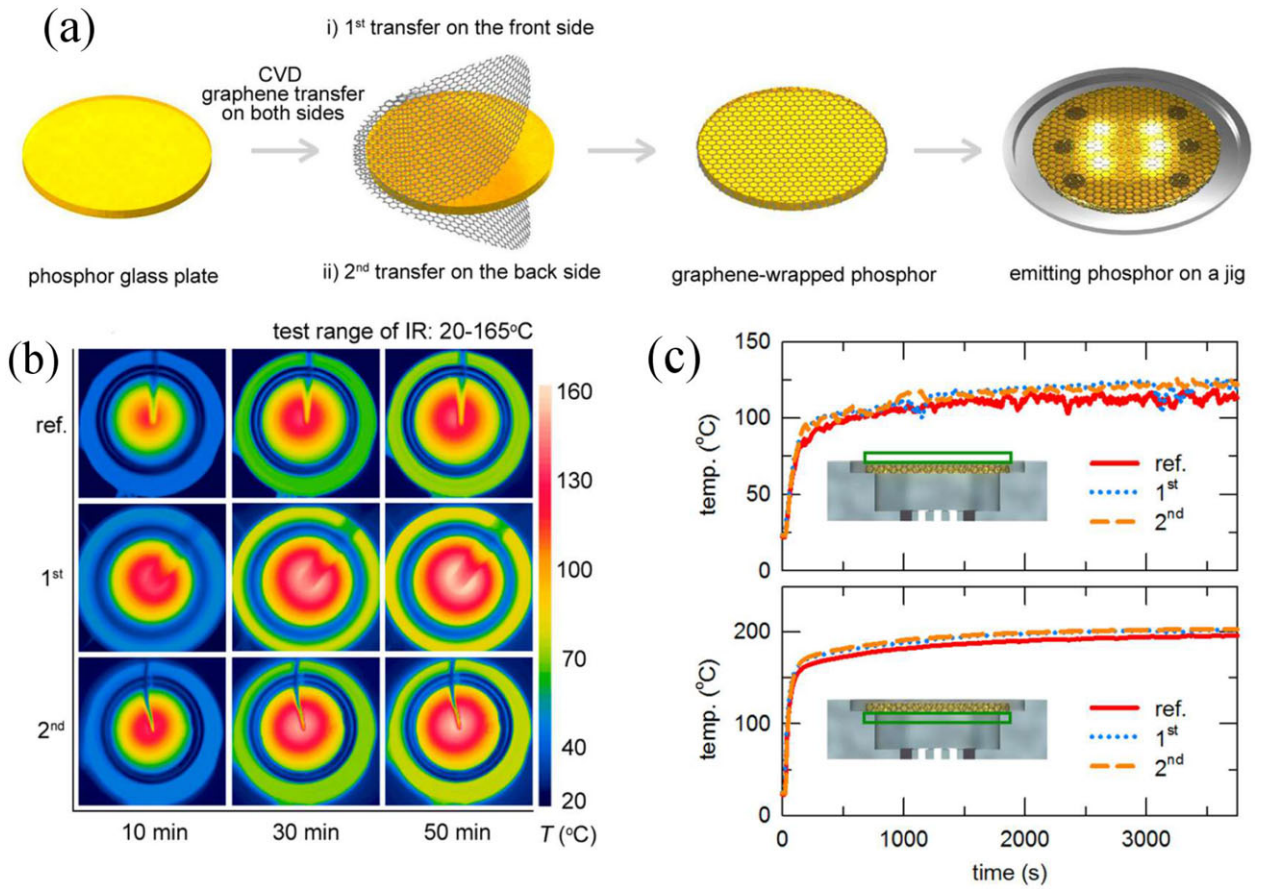

Figure 29. a) Schematic illustration of the preparation of graphene wrapped GC. b) Thermal imaging of the LEDs on state. c) Temperature variations on the top and rear surfaces of GC as the working time prolonged. Reproduced with permission.[140] Copyright 2016, American Chemical Society.

significant in the case of the extremely high input power (e.g., the order of hundreds or thousands watt). Therefore, the effective thermal management for GC during w-LED operation is necessary. At present, there are two ways: one is placing GC plate away from the heat source to form the remote-type GC-based w-LED, and the other one is wrapping the GC with a high thermal-conductivity material.

GC coupled with LED in a remote-type package can partially deliver the thermal management. However, the accumulated heat under a high forward bias current for long-term operation could not be ignored. One promising method to perform better thermal management is wrapping the GC (thermal conductivity of ≈1 W/mK) with transparent graphene (thermal conductivity approaching to 1000 W/mK), as proposed by Kim et al.[140] The single-layer graphene was prepared on a copper foil by a CVD method and then transferred to GC with the aid of PMMA (**Figure 29**a). Compared with bare-GC, the graphene wrapped GC (G-GC) exhibits better color stability as the driving current increases, as well as 20% higher EL intensity. Interestingly, it is found that the graphene effectively drives all the heat accumulated at the center to the periphery of the GC plate and the thermal convection occurs more effectively at the surface of GC close to chip die. A cellular automata simulation was performed to reveal the mechanism of the heat transfer, confirming the heat spreading over the GC surface dissipates effectively into the neighboring air via convection with the aid of graphene wrapping (Figure 29b,c).

6. Summary and Outlook

With the development over ten years, GC has become one of the most promising color converters for high-power w-LED application, exhibiting not only the admirable luminescent properties, but also the excellent resistance to thermal shock from chip die. The preparation strategy of GC has expanded to glass crystallization, low-temperature co-sintering, sol-gel, screen-printing, tape-casting, and SPS. All kinds of up-to-date Eu^{2+}-, Ce^{3+}-, Eu^{3+}-, and Mn^{4+}-activated phosphors and QDs have been incorporated into various glass hosts. In this review article, we described the design and synthesis of GC for w-LED application. The focus was put on the recent progress on the study of relationship between microstructure and optical properties in GC. The microstructure, including phosphor size, phosphor distribution, glass-phosphor interfaces, and pore properties, should be optimized by varying the glass composition and preparation procedure. The optical properties, including transparency, QE, spectral profile, thermal quenching behavior in GC, as well as the luminous performances (LE, CCT, CRI, and ACU) in GC-based w-LEDs, can feed back into the microstructure optimization. Not

just the conventional blue-excited cool w-LED, the blue-excited warm w-LED, UV-excited w-LED, AC-LED, and w-LD have also been realized by utilizing GC as the color converter. Moreover, a considerable progress has been made in optimizing the packaging technique of GC-based w-LED, e.g., the GRIN structure design, geometrical configuration design, secondary optical design and thermal management. Apparently, the easy fabrication, low cost and long-lifetime of GC-based w-LED would become a new-generation indoor/outdoor high-power lighting source.

Looking forward, future work includes but not limits to the following aspects:

- Though the GC-based w-LED technology has become more and more matured, the exploration of new glass system and GC preparation method will never stop the steps. The research priorities would be the chromaticity-tunable GC for high-CRI w-LED, the persistent GC for AC-LED, the ultra-stable GC for w-LD, and the narrowband emissive GC for backlight displays.
- Fundamental issues, including the glass crystallization kinetics, the controllable crystal growth of specific crystallites, the distribution of the doping activators, the manipulation of glass-phosphor interface, should be further studied.
- In view of the subdivision field of w-LED is rapidly expanding, the collaboration between academics and industry should be strengthened to develop different kinds of GC catering to diverse applications.
- The GC preparation and processing techniques should be scaled-up to realize the large-scale production of GC plate.
- The LED technology changes with each passing day, with the chip configuration evolving from the face-up type to the flip- and vertical-type; correspondingly, the power conversion efficiency of blue-LED chip has reached beyond 50%. LE of the GC-based w-LED would be further improved by using these new-type chip configuration. Therefore, the development of new packaging technique for GC should be accelerated to meet up with new requirements in the flip- and vertical-type LED structure.

Acknowledgements

This work was supported by the National Natural Science Foundation of China (11774346, 11674318, 51472242), the National Key R&D Program of China (2016YFB0701003), and the Chunmiao Project of the Haixi Institute of the Chinese Academy of Sciences (CMZX-2017-002).

Conflict of Interest

The authors declare no conflict of interest.

Keywords

glass ceramics, luminescence, optical materials, white light-emitting-diodes

Received: December 26, 2017
Revised: March 15, 2018
Published online:

[1] Z. G. Xia, Q. L. Liu, *Prog. Mater. Sci.* **2016**, *84*, 59.
[2] Z. G. Xia, A. Meijerink, *Chem. Soc. Rev.* **2017**, *46*, 275.
[3] Z. G. Xia, Z. H. Xu, M. Y. Chen, Q. L. Liu, *Dalton Trans.* **2016**, *45*, 11214.
[4] J. Cho, J. H. Park, J. K. Kim, E. F. Schubert, *Laser Photonics Rev.* **2017**, *11*, 201600147.
[5] S. Ye, F. Xiao, Y. X. Pan, Y. Y. Ma, Q. Y. Zhang, *Mat. Sci. Eng. R* **2010**, *71*, 1.
[6] P. Pust, P. J. Schmidt, W. Schnick, *Nat. Mater.* **2015**, *14*, 454.
[7] M. H. Chang, D. Das, P. V. Varde, M. Pecht, *Microelectron. Reliab.* **2012**, *52*, 762.
[8] R. Zhang, H. Lin, Y. L. Yu, D. Q. Chen, J. Xu, Y. S. Wang, *Laser Photonics Rev.* **2014**, *8*, 158.
[9] H. Yoo, Y. Kouhara, H. C. Yoon, S. J. Park, J. H. Oh, Y. R. Do, *RSC Adv.* **2016**, *6*, 111640.
[10] S. Nishiura, S. Tanabe, K. Fujioka, Y. Fujimoto, *Opt. Mater.* **2011**, *33*, 688.
[11] N. A. Wei, T. C. Lu, F. Li, W. Zhang, B. Y. Ma, Z. W. Lu, J. Q. Qi, *Appl. Phys. Lett.* **2012**, *101*, 061902.
[12] A. Lenef, J. Kelso, M. Tchoul, O. Mehl, J. Sorg, Y. Zheng, *Proc. of SPIE*, **2014**, *9190*, 91900C-1.
[13] S. Fujita, S. Tanabe, *Int. J. Appl. Glass Sci.* **2015**, *6*, 356.
[14] S. Fujita, A. Sakamoto, S. Tanabe, *IEEE J. Sel. Top Quant.* **2008**, *14*, 1387.
[15] C. C. Tsai, C. H Chung, J. Wang, W.C. Cheng, M. H. Chen, J. S. Liou, J. K. Chang, Y. C. Hsu, S. C. Huang, C. W. Lee, H. L. Hu, S. B. Huang, J. H. Kuang, W.H. Cheng, *ECTC*, Las Vegas, Nevada, **2010**, p. 700, June 1–4.
[16] Y. K. Lee, J. S. Lee, J. Heo, W. B. Im, W. J. Chung, *Opt. Lett.* **2012**, *37*, 3276.
[17] D. Q. Chen, W. D. Xiang, X. J. Liang, J. S. Zhong, H. Yu, M. Y. Ding, H. W. Lu, Z. G. Ji, *J. Eur. Ceram. Soc.* **2015**, *35*, 859.
[18] G. G. Li, Y. Tian, Y. Zhao, J. Lin, *Chem. Soc. Rev.* **2015**, *44*, 8688.
[19] G. J. Gao, J. X. Wei, Y. Shen, M. Y. Peng, L. Wondraczek, *J. Mater. Chem. C* **2014**, *2*, 8678.
[20] Z. Zhou, N. Zhou, M. Xia, M. Yokoyama, H. T. Hintzen, *J. Mater. Chem. C* **2016**, *4*, 9143.
[21] D. Q. Chen, Y. Zhou, J. S. Zhong, *Rsc Adv.* **2016**, *6*, 86285.
[22] H. Lin, T. Hu, Q. M. Huang, Y. Cheng, B. Wang, J. Xu, J. M. Wang, Y. S. Wang, *Laser Photonics Rev.* **2017**, *11*, 201700148.
[23] T. Hu, H. Lin, Y. Cheng, Q. M. Huang, J. Xu, Y. Gao, J. M. Wang, Y. S. Wang, *J. Mater. Chem. C* **2017**, *5*, 10524.
[24] H. Chen, H. Lin, Q. M. Huang, F. Huang, J. Xu, B. Wang, Z. B. Lin, J. C. Zhou, Y. S. Wang, *J. Mater. Chem. C* **2016**, *4*, 2374.
[25] X. H. He, Y. C. Qiu, S. H. Yang, *Adv. Mater.* **2017**, *29*, 1700775.
[26] N. Karpukhina, R. G. Hill, R. V. Law, *Chem. Soc. Rev.* **2014**, *43*, 2174.
[27] C. Y. Wang, M. Chen, J. H. Chen (eds.), *Glass Making Techniques (in chinese)*, Chemical Industry Press, Beijing **2006**, Ch. 4.
[28] H. Lin, D. Q. Chen, Y. L. Yu, A. P. Yang, Y. S. Wang, *Opt. Lett.* **2011**, *36*, 876.
[29] H. Lin, D. Q. Chen, Y. L. Yu, Z. F. Shan, P. Huang, Y. S. Wang, J. L. Yuan, *J. Appl. Phys.* **2010**, *107*, 103511.
[30] D. Q. Chen, Y. S. Wang, in *Rare-Earth Ions Doped Transparent Oxyfluoride Glass Ceramics*, (Ed. G.S. Murugan), Photonic Glasses and Glass-ceramics, Research Signpost, Kerala, India **2010**, p. 223.
[31] H. Segawa, S. Ogata, N. Hirosaki, S. Inoue, T. Shimizu, M. Tansho, S. Ohki, K. Deguchi, *Opt. Mater.* **2010**, *33*, 170.
[32] F. X. Gan, *J. Non-Cryst. Solids*, **1995**, *184*, 9.
[33] H. Chen, H. Lin, J. Xu, B. Wang, Z. B. Lin, J. C. Zhou, Y. S. Wang, *J. Mater. Chem. C* **2015**, *3*, 8080.
[34] H. Segawa, N. Hirosaki, *J. Ceram. Soc. Jpn.* **2015**, *123*, 452.
[35] L. Yang, M. X. Chen, Z. C. Lv, S. M. Wang, X. G. Liu, S. Liu, *Opt. Lett.* **2013**, *38*, 2240.

[36] F. Y. Wang, Y. Lin, H. L. Shi, W. C. Wang, Z. H. Deng, J. Chen, X. Y. Yuan, Y. G. Cao, *Opt. Express* **2014**, *22*, A1355.
[37] H. Segawa, H. Yoshimizu, N. Hirosaki, S. Inoue, *Sci. Technol. Adv. Mat.* **2011**, *12*, 034407.
[38] B. Y. Zhou, W. Luo, S. Liu, S. J. Gu, M. C. Lu, Y. Zhang, Y. C. Fan, W. Jiang, L. J. Wang, *Acta Mater.* **2017**, *130*, 289.
[39] J. J. Shyu, C. W. Yang, *J. Am. Ceram. Soc.* **2017**, *100*, 1460.
[40] L. Y. Chen, W. C. Cheng, C. C. Tsai, Y. C. Huang, Y. S. Lin, W. H. Cheng, *Opt. Mater. Express* **2014**, *4*, 121.
[41] L. Y. Chen, W. C. Cheng, C. C. Tsai, J. K. Chang, Y. C. Huang, J. C. Huang, W. H. Cheng, *Opt. Express* **2014**, *22*, A671.
[42] A. Herrmann, C. Russel, P. Pachler, *Opt. Mater. Express* **2015**, *5*, 2193.
[43] J. Xu, D. A. Hassan, R. J. Zeng, D. L. Peng, *J. Eur. Ceram. Soc.* **2016**, *36*, 2017.
[44] S. Kim, H. Yie, S. Choi, A. Sung, H. Kim, *Opt. express* **2015**, *23*, A1499.
[45] H. Yie, S. Kim, Y. Kim, H. Kim, *J Non-Cryst Solids* **2017**, *463*, 19.
[46] J. Seo, S. Kim, Y. Kim, F. Iqbal, H. Kim, *J. Am. Ceram. Soc.* **2014**, *97*, 2789.
[47] C. B. Yoon, S. Kim, S. W. Choi, C. Yoon, S. H. Ahn, W. J. Chung, *Opt. Lett.* **2016**, *41*, 1590.
[48] J. Huang, X. J. Liang, W. D. Xiang, M. G. Gong, G. R. Gu, J. S. Zhong, D. Q. Chen, *Mater. Lett.* **2015**, *151*, 31.
[49] T. Nakanishi, S. Tanabe, *IEEE J. Sel. Top. Quant.* **2009**, *15*, 1171.
[50] H. Lin, R. Zhang, D. Q. Chen, Y. L. Yu, A. P. Yang, Y. S. Wang, *J. Mater. Chem. C* **2013**, *1*, 1804.
[51] H. Karimi, Y. T. Zhang, S. Cui, R. H. Ma, G. Li, Q. N. Wang, J. J. Zhao, X. Qiao, J. C. Du, X. P. Fan, *J. Non-Cryst. Solids* **2014**, *406*, 119.
[52] D. Q. Chen, Y. L. Yu, H. Lin, P. Huang, F. Y. Weng, Z. F. Shan, Y. S. Wang, *Opt. Lett.* **2009**, *34*, 2882.
[53] A. Herrmann, A. Simon, C. Russel, *J. Lumin.* **2012**, *132*, 215.
[54] J. Y. Qian, Q. Luo, D. L. Zhao, S. O. Cui, X. S. Qiao, X. P. Fan, X. H. Zhang, *Opt. Mater.* **2012**, *34*, 700.
[55] H. Guo, F. Li, J. J. Li, H. Zhang, *J. Am. Ceram. Soc.* **2011**, *94*, 1651.
[56] F. X. Xin, S. L. Zhao, S. Q. Xu, L. H. Huang, G. H. Jia, D. G. Deng, H. P. Wang, *Opt. Mater.* **2011**, *34*, 85.
[57] R. G. Ye, H. P. Ma, C. Zhang, Y. Q. Gao, Y. J. Hua, D. G. Deng, P. Liu, S. Q. Xu, *J. Alloy Compd.* **2013**, *566*, 73.
[58] S. H. Lee, S. R. Bae, Y. G. Choi, W. J. Chung, *Opt. Mater.* **2015**, *41*, 71.
[59] H. A. Park, Y. K. Lee, W. B. Im, J. Heo, W. J. Chung, *Opt. Mater.* **2015**, *41*, 67.
[60] Y. K. Lee, Y. H. Kim, J. Heo, W. Bin Im, W. J. Chung, *Opt. Lett.* **2014**, *39*, 4084.
[61] K. Han, S. H. Lee, Y. G. Choi, W. B. Im, W. J. Chung, *J. Non-Cryst. Solids* **2016**, *445*, 77.
[62] J. S. Lee, P. Arunkumar, S. Kim, I. J. Lee, H. Lee, W. Bin Im, *Opt. Lett.* **2014**, *39*, 762.
[63] J. S. Lee, S. Unithrattil, S. Kim, I. J. Lee, H. Lee, W. B. Im, *Opt. Lett.* **2013**, *38*, 3298.
[64] I. S. Sohn, S. Unithrattil, W. B. Im, *Acs Appl. Mater. Interfaces* **2014**, *6*, 5744.
[65] E. Kim, S. Unithrattil, I. S. Sohn, S. J. Kim, W. J. Chung, W. B. Im, *Opt. Mater. Express* **2016**, *6*, 804.
[66] Y. H. Kim, P. Arunkumar, W. Bin Im, *Ceram. Int.* **2015**, *41*, 5200.
[67] S. Kim, H. Park, W. B. Im, J. Heo, J. Choi, W. Chung, *J. Am. Ceram. Soc.* **2017**, *XX*, XX. https://doi.org/10.1111/jace.15043.
[68] S. Yi, W. J. Chung, J. Heo, *J. Am. Ceram. Soc.* **2014**, *97*, 342.
[69] S. Yi, W. J. Chung, J. Heo, *J. Am. Ceram. Soc.* **2017**, *100*, 2378.
[70] C. C. Tsai, *Int. J. Photoenergy*, **2014**, *XX*, 407239.
[71] G. Liu, Z. F. Tian, Z. H. Chen, H. Z. Wang, Q. H. Zhang, Y. G. Li, *Opt. Mater.* **2015**, *40*, 63.
[72] J. K. Deng, W. Li, H. R. Zhang, Y. L. Liu, B. F. Lei, H. M. Zhang, L. S. Liu, X. Bai, H. Y. Luo, H. Z. Liu, W. R. Liu, J. Wang, *Adv. Opt. Mater.* **2017**, *5*, 1600910.
[73] Q. Q. Zhu, X. J. Wang, L. Wang, N. Hirosaki, T. Nishimura, Z. F. Tian, Q. Li, Y. Z. Xu, X. Xu, R. J. Xie, *J. Mater. Chem. C* **2015**, *3*, 10761.
[74] Q. Q. Zhu, X. Xu, L. Wang, Z. F. Tian, Y. Z. Xu, N. Hirosaki, R. J. Xie, *J. Alloy Compd.* **2017**, *702*, 193.
[75] X. J. Zhang, J. B. Yu, J. Wang, C. B. Zhu, J. H. Zhang, R. Zou, B. F. Lei, Y. L. Liu, M. M. Wu, *ACS Appl. Mater. Interfaces* **2015**, *7*, 28122.
[76] X. J. Zhang, J. B. Yu, J. Wang, B. F. Lei, Y. L. Liu, Y. J. Cho, R. J. Xie, H. W. Zhang, Y. R. Li, Z. F. Tian, Y. Li, Q. Su, *ACS Photonics* **2017**, *4*, 986.
[77] H. Segawa, N. Hirosaki, S. Ohki, K. Deguchi, T. Shimizu, *Opt. Mater.* **2013**, *35*, 2677.
[78] H. Segawa, N. Hirosaki, S. Ohki, K. Deguchi, T. Shimizu, *Opt. Mater.* **2015**, *42*, 399.
[79] H. Segawa, N. Hirosaki, *Appl. Opt.* **2015**, *54*, 8727.
[80] B. Wang, H. Lin, J. Xu, H. Chen, Y. S. Wang, *ACS Appl. Mater. Interfaces* **2014**, *6*, 22905.
[81] B. Wang, H. Lin, F. Huang, J. Xu, H. Chen, Z. B. Lin, Y. S. Wang, *Chem. Mater.* **2016**, *28*, 3515.
[82] Z. B. Lin, H. Lin, J. Xu, F. Huang, H. Chen, B. Wang, Y. S. Wang, *J. Eur. Ceram. Soc.* **2016**, *36*, 1723.
[83] H. Lin, B. Wang, J. Xu, R. Zhang, H. Chen, Y. L. Yu, Y. S. Wang, *ACS Appl. Mater. Interfaces* **2014**, *6*, 21264.
[84] D. Q. Chen, Y. Chen, *Ceram. Int.* **2014**, *40*, 15325.
[85] J. S. Zhong, D. Q. Chen, W. G. Zhao, Y. Zhou, H. Yu, L. F. Chen, Z. G. Ji, *J. Mater. Chem. C* **2015**, *3*, 4500.
[86] Y. Zhou, D. Q. Chen, W. D. Tian, Z. G. Ji, *J. Am. Ceram. Soc.* **2015**, *98*, 2445.
[87] J. S. Zhong, D. Q. Chen, Y. Zhou, Z. Y. Wan, M. Y. Ding, Z. G. Ji, *J. Eur. Ceram. Soc.* **2016**, *36*, 1705.
[88] J. S. Zhong, D. Q. Chen, Y. Zhou, Z. Y. Wan, M. Y. Ding, W. F. Bai, Z. G. Ji, *Dalton T.* **2016**, *45*, 4762.
[89] D. Q. Chen, Y. Zhou, W. Xu, J. S. Zhong, Z. G. Ji, W. D. Xiang, *J. Mater. Chem. C* **2016**, *4*, 1704.
[90] D. Q. Chen, W. Xu, Y. Zhou, J. S. Zhong, S. C. Li, *J. Mater. Chem. C* **2017**, *5*, 738.
[91] J. S. Zhong, W. Xu, Q. L. Chen, S. Yuan, Z. G. Ji, D. Q. Chen, *Dalton T.* **2017**, *46*, 9959.
[92] D. Q. Chen, S. Yuan, X. Y. Li, W. Xu, *RSC Adv.* **2017**, *7*, 36168.
[93] X. Q. Xiang, B. Wang, H. Lin, J. Xu, J. M. Wang, T. Hu, Y. S. Wang, *J. Eur. Ceram. Soc.* **2017**, *XX*, XX. DOI: https://doi.org/j.jeurceramsoc.2017.10.013
[94] M. G. Gong, X. J. Liang, Y. Y. Wang, H. H. Xu, L. Zhang, W. D. Xiang, *J. Alloy Compd.* **2016**, *664*, 125.
[95] J. Huang, X. L. Hu, J. J. Shen, D. L. Wu, C. F. Yin, R. Xiang, C. Yang, X. J. Liang, W. D. Xiang, *Crystengcomm* **2015**, *17*, 7079.
[96] C. Y. Ma, Y. G. Cao, X. F. Shen, Z. C. Wen, R. Ma, J. Q. Long, X. Y. Yuan, *Opt. Mater.* **2017**, *69*, 105.
[97] S. M. Wang, X. Chen, M. X. Chen, H. Zheng, H. R. Yang, S. Liu, *Appl. Opt.* **2014**, *53*, 8492.
[98] Y. Peng, S. M. Wang, R. X. Li, H. Li, H. Cheng, M. X. Chen, S. Liu, *Appl. Opt.* **2016**, *55*, 4933.
[99] Y. Peng, H. Cheng, Z. Chen, M. X. Chen, R. X. Li, *17 ICEPT*, Wuhan **2016**, p. 61, Aug 16–19.
[100] R. X. Li, H. Li, Y. Peng, H. Cheng, Z. Chen, M. X. Chen, *17 ICEPT*, Wuhan **2016**, p. 94, Aug 16–19.
[101] Y. Peng, H. Cheng, Z. Chen, M. X. Chen, H. Wang, *17 ICEPT*, Wuhan **2016**, p. 65, Aug 16–19.
[102] Y. Peng, R. X. Li, H. Cheng, Z. Chen, H. Li, M. X. Chen, *J. Alloy Compd.* **2017**, *693*, 279.
[103] Y. Peng, R. X. Li, H. Cheng, Z. Chen, M. X. Chen, *13 SSLChina*, Beijing **2016**, p. 17.
[104] Y. Peng, X. Guo, R. X. Li, H. Cheng, M. X. Chen, *Appl. Opt.* **2017**, *56*, 3270.

[105] Y. Peng, R. X. Li, S. M. Wang, Z. Chen, L. Nie, M. X. Chen, *IEEE T. Electron. Dev.* **2017**, *64*, 1114.
[106] Y. Peng, R. X. Li, X. Guo, H. Zheng, M. X. Chen, *Appl. Opt.* **2016**, *55*, 8189.
[107] S. H. Ahn, Y. H. Nam, K. Han, W. B. Im, K. Y. Cho, W. J. Chung, *J. Am. Ceram. Soc.* **2017**, *100*, 1280.
[108] J. S. Kim, O. H. Kwon, J. W. Jang, S. H. Lee, S. J. Han, J. H. Lee, Y. S. Cho, *ACS Comb. Sci.* **2015**, *17*, 234.
[109] O. H. Kwon, J. S. Kim, J. W. Jang, H. Yang, Y. S. Cho, *Opt. Mater. Express* **2016**, *6*, 938.
[110] B. H. Kim, J. Hwang, Y. J. Lee, J. H. Kim, D. W. Jeon, M. J. Lee, *Opt. Eng.* **2016**, *55*, 085103.
[111] B. H. Kim, J. Hwang, Y. J. Lee, J. H. Kim, D. W. Jeon, M. J. Lee, *J. Kor. Ceram. Soc.* **2016**, *53*, 381.
[112] R. Zhang, B. Y. Wang, W. F. Zhu, C. J. Li, H. Wang, *J. Alloy. Compd.* **2017**, *720*, 340.
[113] Y. Zhuo, H. Li, X. J. Xu, M. X. Chen, D. H. Xiong, Y. T. Long, S. Chen, R. X. Li, Z. R. Liu, *J. Non-Cryst. Solids* **2017**, *471*, 215.
[114] R. Cao, L. C. Wu, X. X. Di, P. Z. Li, G. C. Hu, X. J. Liang, W. D. Xiang, *Opt. Mater.* **2017**, *70*, 92.
[115] R. Xiang, X. J. Liang, Q. Y. Xi, Z. F. Yuan, C. R. Chen, W. D. Xiang, *Ceram. Int.* **2016**, *42*, 19276.
[116] R. Xiang, X. J. Liang, P. Z. Li, X. X. Di, W. D. Xiang, *Chem. Eng. J.* **2016**, *306*, 858.
[117] C. Yang, X. J. Liang, X. X. Di, P. Z. Li, G. C. Hu, R. Cao, W. D. Xiang, *Ceram. Int.* **2016**, *42*, 14526.
[118] S. Lin, M. Y. Chen, Z. W. Wang, Y. J. Zhang, R. R. Yuan, X. J. Liang, W. D. Xiang, Y. Q. Zhou, *Chem. Eng. J.* **2017**, *324*, 194.
[119] H. Segawa, S. Samitsu, N. Hirosaki, *Int. J. Appl. Glass Sci.* **2017**, *8*, 247.
[120] K. Yoshimura, H. Fukunaga, M. Izumi, M. Harada, K. Takahashi, H. Segawa, R. J. Xie, N. Hirosaki, *Jpn. J. Appl. Phys.* **2017**, *56*, 060302.
[121] S. Nakajima, H. Segawa, S. Yanagida, A. Yasumori, N. Hirosaki, *J. Ceram. Soc. Jpn.* **2013**, *121*, 361.
[122] S. Fujita, S. Yoshihara, A. Sakamoto, S. Yamamoto, S. Tanabe, *Proc. of SPIE*, **2005**, *5941*, 594111.
[123] S. Tanabe, S. Fujita, S. Yoshihara, A. Sakamoto, S. Yamamoto, *Proc. of SPIE*, **2005**, *5941*, 594112.
[124] S. Fujita, Y. Umayahara, S. Tanabe, *J. Ceram. Soc. Jpn.* **2010**, *118*, 128.
[125] S. Fujita, S. Tanabe, *Jpn. J. Appl. Phys.* **2009**, *48*, 120210.
[126] J. Wang, C. C. Tsai, W. C. Cheng, M. H. Chen, C. H. Chung, W. H. Cheng, *IEEE J. Sel. Top. Quant.* **2011**, *17*, 741.
[127] C. C. Tsai, W. C. Cheng, J. K. Chang, L. Y. Chen, J. H. Chen, Y. C. Hsu, W. H. Cheng, *J. Disp. Technol.* **2013**, *9*, 427.
[128] American National Standards Institute. ANSI_NEMA_ANSLG C *78*.377.
[129] C. W. Yeh, Y. Li, J. Wang, R. S. Liu, *Opt. Express* **2012**, *20*, 18031.
[130] J. J. Wierer, J. Y. Tsao, D. S. Sizov, *Laser Photonics Rev* **2013**, *7*, 963.
[131] H. Lin, T. Hu, Q. M. Huang, Y. Cheng, B. Wang, J. Xu, J. M. Wang, Y. S. Wang, *Laser Photonics Rev* **2017**, *11*, 1700148.
[132] M. Anandan, *J. Soc. Inf. Disp.* **2008**, *16*, 287.
[133] R. J. Xie, N. Hirosaki, T. Takeda, *Appl. Phys. Express*, **2009**, *2*, 022401.
[134] B. Ai, C. Liu, J. Wang, J. Xie, J. J. Han, X. J. Zhao, *J. Am. Ceram. Soc.*, **2016**, *99*, 2875.
[135] X. X. Di, Z. M. Hu, J. T. Jiang, M. L. He, L. Zhou, W. D. Xiang, X. J. Liang, *Chem. Commun.*, **2017**, *53*, 11068.
[136] L. Y. Chen, J. K. Chang, Y. R. Wu, W. C. Cheng, J. H. Chen, C. C. Tsai, W. H. Cheng, *J. Disp. Technol.* **2013**, *9*, 441.
[137] H. R. Yang, M. X. Chen, S. M. Wang, *16 ICEPT*, Changsha **2015**, p. 1448, Aug 11–14.
[138] S. M. Wang, Y. Peng, R. X. Li, M. X. Chen, S. Liu, *CSTIC*, Mar 13–14, Shanghai **2016**.
[139] S. M. Wang, X. Chen, M. X. Chen, Z. L. Hao, H. R. Yang, S. Liu, *16 ICEPT*, Changsha **2015**, p. 432, Aug 11–14.
[140] E. Kim, H. W. Shim, S. Unithrattil, Y. H. Kim, H. Choi, K. J. Ahn, J. S. Kwak, S. Kim, H. Yoon, W. Bin Im, *ACS Nano* **2016**, *10*, 238.